Identification of *Pik3ca* mutation as a genetic driver of prostate cancer that cooperates with *Pten* loss to accelerate progression and castration-resistant growth

Helen B. Pearson[1,2,3], Jason Li[1,2], Valerie S. Meniel[3], Christina M. Fennell[1], Paul Waring[4], Karen G. Montgomery[1], Richard J. Rebello[1,6], Arthi A. Macpherson[7], Sarah Koushyar[3], Luc Furic[1,2,6], Carleen Cullinane[1,2], Richard W. Clarkson[3], Matthew J. Smalley[3], Kaylene J. Simpson[2,7], Toby J. Phesse[3], Peter R. Shepherd[8,9], Patrick O. Humbert[1,2,4,5,10], Owen J. Sansom[11,12] and Wayne A. Phillips[1,2,13]

Affiliations: [1]Peter MacCallum Cancer Centre, Melbourne, Victoria, 3000, Australia. [2]The Sir Peter MacCallum Department of Oncology, The University of Melbourne, Parkville, Victoria, 3010, Australia. [3]European Cancer Stem Cell Research Institute, Haydn Ellis Building, Cardiff University, Cardiff, CF24 4HQ, UK. [4]Department of Pathology, The University of Melbourne, Parkville, Victoria, 3010, Australia. [5]Department of Biochemistry and Genetics, La Trobe Institute for Molecular Science, La Trobe University, Bundoora, Victoria, 3086, Australia. [6]Department of Anatomy and Developmental Biology, Monash University, Clayton, Victoria, Australia. [7]Victorian Centre for Functional Genomics, ACRF RPPA Platform, Peter MacCallum Cancer Centre, Melbourne, Victoria, 3000, Australia, [8]Maurice Wilkins Centre for Molecular Biodiscovery, The University of Auckland, Auckland, New Zealand. [9]Department of Molecular Medicine and Pathology, The University of Auckland, Auckland 1042, New Zealand. [10]Department of Biochemistry and Molecular Biology, The University of Melbourne, Parkville, Victoria, 3010, Australia [11]CRUK Beatson Institute, Garscube Estate, Switchback Road, Glasgow. G61 1BD, UK. [12]Institute of Cancer Sciences, University of Glasgow, Garscube Estate, Switchback Road, Glasgow. G61 1BD, UK. [13]Department of Surgery (St. Vincent's Hospital), The University of Melbourne, Parkville, Victoria, 3010, Australia.

Conflict of interest statement: The authors declare no potential conflicts of interest.

Running Title: *Pik3ca* mutation drives prostate cancer

Keywords: Castration-resistant prostate cancer (CRPC), PI3K, PIK3CA, PTEN, p110α

Financial Support: This work was generously supported by a Prostate Cancer Foundation of Australia (PCFA) concept grant (#CG 1611) and a National Health and Medical Research Council of Australia (NHMRC) project grant (#1080491) awarded to W.A.P, and a Peter MacCallum Cancer Foundation concept grant (#1520) awarded to H.B.P. H.B.P is supported by a Marie Skłodowska Curie Actions/Sêr Cymru II/Horizons 2020 COFUND fellowship (#663830-CU-041). T.J.P is supported by a Capital Medical University/Cardiff University Fellowship. L.F. is supported by the Department of Health and Human Services acting through the Victorian Cancer Agency (MCRF16007). P.O.H is supported by a NHMRC Senior Research Fellowship (#1079133). The Victorian Centre for Functional Genomics (VCFG) and the Reverse Phase Protein Array (RPPA) platform (K.J.S.) is funded by the Australian Cancer Research Foundation (ACRF), the Australian Phenomics Network (APN) through funding from the Australian Government's National Collaborative Research Infrastructure Strategy (NCRIS) program, the Peter MacCallum Cancer Foundation and the University of Melbourne Collaborative Research Infrastructure Program.

Corresponding author: Dr Helen Pearson, European Cancer Stem Cell Research Institute, Haydn Ellis Building, Cardiff University, Cardiff, CF24 4HQ, UK. Tel: +44 (0)2920-688-517. Email: PearsonH2@cardiff.ac.uk

Abstract

Genetic alterations that potentiate PI3K signalling are frequent in prostate cancer, yet how different genetic drivers of the PI3K cascade contribute to prostate cancer is unclear. Here, we report *PIK3CA* mutation/amplification correlates with poor prostate cancer patient survival. To interrogate the requirement of different PI3K genetic drivers in prostate cancer, we employed a genetic approach to mutate *Pik3ca* in mouse prostate epithelium. We show *Pik3ca*^{H1047R} mutation causes p110α-dependent invasive prostate carcinoma *in-vivo*. Furthermore, we report *PIK3CA* mutation and *PTEN* loss co-exist in prostate cancer patients, and can cooperate *in-vivo* to accelerate disease progression via AKT-mTORC1/2 hyperactivation. Contrasting single mutants that slowly acquire castration-resistant prostate cancer (CRPC), concomitant *Pik3ca* mutation and *Pten* loss caused *de-novo* CRPC. Thus, *Pik3ca* mutation and *Pten* deletion are not functionally redundant. Our findings indicate that *PIK3CA* mutation is an attractive prognostic indicator for prostate cancer that may cooperate with *PTEN* loss to facilitate CRPC in patients.

Statement of significance

We show *PIK3CA* mutation correlates with poor prostate cancer prognosis and causes prostate cancer in mice. Moreover, *PIK3CA* mutation and *PTEN* loss co-exist in prostate cancer, and can cooperate *in-vivo* to accelerate tumorigenesis and facilitate CRPC. Delineating this synergistic relationship may present new therapeutic/prognostic approaches to overcome castration/PI3K-AKT-mTORC1/2 inhibitor resistance.

Introduction

Prostate cancer is the second most common male cancer-related death world-wide, emphasizing the failure of mainstay therapeutic regimens to treat advanced disease(1). A pivotal constraint for prostate cancer research is the lack of diverse *in vivo* models that accurately reflect the clinic. Expanding the range of prostate cancer models that display key clinicopathological characteristics is vital to; (i) delineate the complex molecular mechanisms underpinning prostate cancer, (ii) identify novel prognostic markers and therapeutic targets, and (iii) accurately establish the efficacy of novel therapies that are urgently needed in the clinic.

Class 1A phosphatidylinositol 3-kinases (PI3Ks) are heterodimers consisting of a regulatory subunit encoded by *PIK3R1* (p85α/p55α/p50α), *PIK3R2* (p85β) or *PIK3R3* (p85γ), and a catalytic subunit encoded by *PIK3CA* (p110α), *PIK3CB* (p110β) or *PIK3CD* (p110δ)(2,3). Upon activation of receptor tyrosine kinases (RTKs), G-protein coupled receptors (GPCRs) or RAS, PI3K is recruited to the membrane. Here, PI3K catalyses the generation of the second messenger phosphatidylinositol(3,4,5)trisphosphate (PIP_3), which recruits the serine threonine kinases AKT (Protein kinase B, PKB) and Phosphoinositide-dependent kinase-1 (PDK1) to the membrane, as well as a plethora of other PIP_3 binding proteins (4). The first identified, and most well studied, PIP_3 effector is AKT(4). PDK1 phosphorylates AKT at Thr308, leading to phosphorylation of downstream targets including Tuberous Sclerosis Complex 2 (TSC2) that activates mTOR complex-1 (mTORC1) to promote proliferation, survival and migration(2,3). Phosphorylation of AKT at both Ser473 and Thr308 is required for the full activation of AKT, and has been linked to co-activation of the mTORC1 and mTOR complex-2 (mTORC2) pathways(5). Key substrates of mTORC2 include AKT at Ser473(5), and serum/glucocorticoid regulated kinase-1 (SGK1), which phosphorylates and inactivates the metastasis suppressor N-

Myc down-regulated gene-1 (NDRG1/DRG1/CAP43)(6). AKT dephosphorylation by PH domain leucine-rich repeat protein phosphatase (PHLPP) at Ser473 and Protein phosphatase 2 (PP2A) at Thr308 deactivate AKT(5). The fine tuning of AKT phosphorylation levels mediates AKT pathway activity and subsequent cellular events. In addition, the tumor suppressor Phosphatase and tensin homolog (PTEN) serves to negatively regulate the PI3K cascade by catalysing the dephosphorylation of PIP_3 to phosphatidylinositol 4,5-bisphosphate (PIP_2). PTEN also mediates lipid phosphatase-independent tumor suppressor activities via its protein phosphatase domain(2).

PI3K pathway hyperactivation is invariably associated with prostate cancer progression in the clinic, thus presenting an attractive therapeutic target. Indeed, loss of *PTEN*, a negative regulator of the PI3K pathway, is estimated to occur in 40-50% of prostate cancer patients(7,8). However, PI3K pathway hyperactivation can occur via a range of mechanisms (e.g. *PIK3CA* oncogenic mutation) that can independently influence downstream signaling events. We sought to determine if genetic drivers of the PI3K pathway that are present in prostate cancer, but have not been investigated previously, can also contribute to prostate cancer initiation/progression. To this end we generated a new, clinically relevant genetically modified mouse model harbouring a heterozygous activating mutation in *Pik3ca* specifically within prostate epithelial cells, and compared prostate histopathology with the well-characterised *Pten*-deleted mouse model of prostate cancer(9). Overall, our findings emphasize the prognostic value of PI3K genetic drivers to better inform personalised therapy design.

Results

PIK3CA mutation/amplification correlates with advanced prostate cancer progression.

PIK3CA oncogenic mutation and amplification, which may increase p110α PI3K catalytic

activity, are frequently detected in human cancers (10-13). To better understand the frequency of *PIK3CA* alterations in prostate cancer, we analysed nine prostate cancer genomic datasets for *PIK3CA* mutations and gene amplification(14). Our analysis shows that *PIK3CA* mutations occur in up to 4% of prostate cancer patients, while *PIK3CA* copy number gain/amplification occurs in as many as 62% of cases (Fig.1A, Supplementary Table 1). *PIK3CA* mutations were predominantly nucleotide missense substitutions (87.5%, Supplementary Fig.1A) within the helical (44.1%) and kinase (20.6%) domains, and previously reported hotspot mutations in exon 9 (E542K, E545K) and 20 (H1047R)(10-12,15) were most frequent (Fig.1B). Notably, the majority of *PIK3CA* mutations observed (83%, 19/23) have been previously detected in prostate or non-prostate malignancies(12,13,15,16), and are reported to increase p110α activity(12,15-18) (Fig.1B).

To determine if *PIK3CA* mutation/amplification correlates with prostate cancer progression, we analysed the TCGA provisional prostate cancer dataset (Supplementary Table 2). Our analysis revealed that *PIK3CA* mutation and copy number gain/amplification frequency significantly correlates with poor prostate cancer survival, regional lymph node metastasis, and a higher pT category and Gleason grade (Fig.1C, Supplementary Table 3), resembling *PTEN* loss (Supplementary Fig.1B, Supplementary Table 4).

Co-expression analysis within the nine prostate cancer datasets analysed revealed that 39.4% (13/33 patients) of *PIK3CA* mutation carriers also harboured *PTEN* mutation or copy number loss, indicating that *PIK3CA* mutant prostate cancer patients have a high frequency of co-existent *PTEN* deleterious genetic alterations, consistent with ovarian, breast, endometrial, and colorectal cancer studies(11,19,20). Interestingly, 47.5% (96/202) of prostate cancer patients with *PIK3CA* amplification/gain also carried a *PTEN* mutation or copy number loss. Moreover,

statistical analysis of the larger TCGA provisional dataset revealed a significant tendency towards *PIK3CA* mutation/amplification/gain and *PTEN* mutation/loss co-occurrence in prostate cancer patients (P<0.001, Fisher's exact test, Log odds ratio = 0.916). Together, these findings suggest that *PIK3CA* mutation/amplification/gain play an oncogenic role during prostate cancer and indicate that p110α gain-of-function and *PTEN* loss may cooperate to promote prostate cancer growth.

***Pik3ca*^{H1047R} mutation in mouse prostate epithelium causes locally invasive prostate carcinoma.** To delineate the oncogenic role of a clinically relevant *PIK3CA* mutation within the prostate, we inter-crossed mice that harbor a conditional latent H1047R mutation in *Pik3ca* to the *PBiCre* transgenic line. Using an exon-switch Cre-LoxP approach, expression of *Pik3ca*^{H1047R} was driven specifically within the prostate following *PBiCre*-mediated excision of the floxed wild-type (Wt) *Pik3ca* exon 20 and subsequent expression of a latent downstream mutant exon 20(11,21). Recombination was confirmed by sequencing and allele-specific PCR analysis of cDNA isolated from the prostate glands of *PBiCre*$^{+/-}$*;Pik3ca*$^{+/+}$ and *PBiCre*$^{+/-}$*;Pik3ca*$^{+/Lat\text{-}H1047R}$ mice, hereafter referred to as *Wt* and *Pik3ca*$^{+/HR}$ respectively (Supplementary Fig.2A-B). Histological analysis of *Wt* and *Pik3ca*$^{+/HR}$ prostate lobes revealed no gross phenotype in *Wt* mice, whereas *Pik3ca*$^{+/HR}$ cohorts displayed a progressive malignant phenotype. *Pik3ca*$^{+/HR}$ mice developed multifocal simple and/or cribriform hyperplasia in all prostate lobes by 100 d and homogeneous, locally invasive prostate carcinoma by 300–400 d (dorsolateral lobe: Fig.2A-B, and ventral/anterior lobes: Supplementary Fig.2C-E, Supplementary Table 5). Invasion was confirmed by the absence of smooth muscle actin (SMA) staining by immunohistochemistry (IHC) (Supplementary Fig.2F). *Pik3ca*$^{+/HR}$ prostate carcinomas were predominantly dysplastic/mucinous and reactive stroma and immune infiltrate were evident (Fig.2A; 300-400 d, Supplementary Fig.2C). Taken together, these data

demonstrate that heterozygous *Pik3ca*^{H1047R} oncogenic mutation is sufficient to cause invasive prostate cancer in mice, and to our knowledge is the first example of a mono-allelic mutation driving invasive prostate cancer growth *in vivo*.

To determine if the genetic driver of the PI3K cascade influences prostate tumorigenesis and/or malignant progression, we compared our novel *Pik3ca*$^{+/HR}$ prostate cancer model with the well-characterised *Pten*-deleted mouse model of prostate cancer(9). To this end, we generated age-matched cohorts of *PBiCre*$^{+/-}$;*Pten*$^{fl/fl}$ mice (denoted *Pten*$^{fl/fl}$) deficient for both copies of *Pten* within prostate epithelial cells and compared the phenotype on the same genetic background. In contrast to *Pik3ca*$^{+/HR}$ mice, we observed early onset of hyperplastic lesions at 56 d and rapid tumor progression from prostate intraepithelial neoplasia (PIN) to locally invasive carcinoma in *Pten*$^{fl/fl}$ mice by 200 d (Fig.2A-B, Supplementary Fig.2C-E, Supplementary Table 5). Furthermore, *Pten*$^{fl/fl}$ prostate tumor burden was significantly greater and more heterogenous than the *Pik3ca*$^{+/HR}$ model (Fig.2A/C), as carcinosarcomas were also present by 300 d in 29% of the cohort (2/7). However, metastasis to the liver, lung, lymph nodes or bone was not detected in either model. *Pten*$^{fl/fl}$ mice were also prone to seminal vesicle neoplasia, urethra neoplasia and adrenal pheochromocytoma that were rare, or absent, in *Pik3ca*$^{+/HR}$ mice (Supplementary Table 5). These findings indicate that relative to the *Pik3ca*$^{+/HR}$ model, early disease onset, and potentially accelerated progression, contribute to the earlier emergence of invasive carcinoma in *Pten*$^{fl/fl}$ mice.

To investigate if *Pten* bi-allelic loss accelerates prostate tumor growth compared to *Pik3ca*$^{+/HR}$-driven prostate cancer, we performed and quantitated IHC to detect the S-phase proliferation marker PCNA. *Pik3ca*$^{+/HR}$ prostate disease (100–400 d) showed a significant increase in the number of PCNA-positive proliferating cells compared to *Wt* controls, however a clear

proliferation advantage was evident in *Pten*$^{fl/fl}$ mice between 56–200 d (Fig.3A-B). Furthermore, significantly more PCNA-positive cells were detected in *Pten*$^{fl/fl}$ prostate hyperplasia compared to *Pik3ca*$^{+/HR}$ hyperplastic lesions (Supplementary Fig.2G), indicating this is an early phenomenon during disease progression. These data show that increased proliferation in *Pten*$^{fl/fl}$ mice facilitates accelerated prostate cancer progression compared to *Pik3ca*$^{+/HR}$ mice. Notably, apoptosis evasion is not likely to contribute to accelerated disease progression in *Pten*$^{fl/fl}$ mice, as the number of cleaved-caspase-3 (CC3)-positive apoptotic cells was largely increased in *Pten*$^{fl/fl}$ prostate epithelium compared to age-matched *Pik3ca*$^{+/HR}$ mutants (Supplementary Fig.3A-B). IHC analysis to detect prostate basal and luminal cell markers cytokeratin-5, (CK5) and cytokeratin-8 (CK8) respectively, revealed that, unlike *Pten*$^{fl/fl}$ prostate tumors, *Pik3ca*$^{+/HR}$-driven tumors are predominantly comprised of luminal epithelial cells and rarely display expansion/mislocalization of the CK5-positive basal cell population (Supplementary Fig.3C). Taken together these data show that while a single *Pik3ca* H1047R activating mutation predisposes to murine prostate cancer, like bi-allelic loss of *Pten*, these two genetic drivers of the PI3K cascade do not completely phenocopy. Overall, these findings suggest that *Pik3ca* oncogenic mutation and *Pten* loss may drive prostate tumor phenotypes via distinct molecular mechanisms, which could present novel therapeutic targets.

***Pik3ca* mutation and *Pten* loss stimulate mTORC1 signaling to promote prostate tumorigenesis and facilitate malignant progression in mice.** Given that both *Pten* deletion and *Pik3ca* oncogenic mutations can activate PI3K signaling, the phenotypic differences observed between the genetic drivers could reflect differential activation of the PI3K cascade. To determine if PTEN tumor suppressive function is maintained in the *Pik3ca*$^{+/HR}$ model, we performed IHC to detect PTEN. We observed uniform membranous PTEN staining in *Wt* prostate epithelium and *Pik3ca*$^{+/HR}$ tumors, whereas PTEN-positive cells were absent in *Pten*$^{fl/fl}$

prostate tumors, consistent with bi-allelic *Pten* ablation (Fig.3C). To determine if PTEN impairs effector cascades downstream of PI3K in the *Pik3ca*$^{+/HR}$ model to delay prostate tumorigenesis and progression, we evaluated AKT activation and the status of the PI3K downstream mechanistic target of rapamycin (mTOR) effector cascades. mTOR is a serine/threonine kinase that forms part of two distinct complexes; mTORC1 and mTORC2. We show that the number of prostate epithelial cells displaying activation of AKT via Thr308 phosphorylation at the cell membrane, is significantly increased in *Pik3ca*$^{+/HR}$ and *Pten*$^{fl/fl}$ prostate carcinoma compared to *Wt* controls (Fig.3C-D), indicating that both PI3K genetic drivers stimulate mTORC1 signaling to promote tumor growth. In support, the proportion of cells displaying phosphorylation of well-known downstream mTORC1 targets, namely the ribosomal protein S6 (RPS6) at Ser235/236 that regulates cell size and proliferation and 4e-binding protein 1 (4E-BP1) at Thr37/46 that mediates translational machinery, were also significantly elevated in both models (Fig.3C, E-F). Our analysis of the number of p-AKT (Thr308), p-RPS6 and p-4E-BP1 positive cells in *Pten*$^{fl/fl}$ and *Pik3ca*$^{+/HR}$ hyperplastic lesions also revealed that mTORC1 signaling upregulation occurs pre-malignancy (Supplementary Fig.3D-G). Of note, the number of p-RPS6 and p-4E-BP1 positive cells were comparable in *Pik3ca*-mutated and *Pten*-deleted hyperplastic lesions and advanced tumors, despite significantly more p-AKT (Thr308) positive cells being detected in the *Pten*$^{fl/fl}$ model, suggesting that p-AKT Thr308 independent phosphorylation of RPS6 and p4E-BP1 may occur, or that the partial increase in p-AKT Thr308 in *Pik3ca*$^{+/HR}$ tumors is sufficient to sustain p-RPS6 and p-4E-BP1 signaling. Taken together, these data indicate that both *Pik3ca* H1047R oncogenic mutation and *Pten* bi-allelic loss stimulate mTORC1 signaling to facilitate prostate tumor formation and progression, and that PTEN-mediated tumor suppressive functions do not impair mTORC1 downstream signaling in the context of *Pik3ca* mutation.

Relative to *Pik3ca* mutation, *Pten* deletion augments mTORC2 signaling to further promote prostate tumor formation and progression in mice. Since activation of the mTORC1 downstream targets was comparable between *Pik3ca*$^{+/HR}$ and *Pten*$^{fl/fl}$ prostate cancer models, we reasoned that the early onset and accelerated progression observed in the *Pten*$^{fl/fl}$ model may be attributable to mTORC2 signaling. To investigate this, we performed and quantitated IHC in *Pik3ca*$^{+/HR}$ and *Pten*$^{fl/fl}$ prostate carcinomas to detect the phosphorylation of two mTORC2 targets; AKT at Ser473 and NDRG1 at Thr346. We show that the number of p-AKT Ser473 and p-NDRG1 Thr346 positive cells was significantly increased in *Pten*$^{fl/fl}$ prostate tumors compared to the *Pik3ca*$^{+/HR}$ model and *Wt* controls (Fig.3C,G-H). Similar results were observed when comparing hyperplastic lesions (Supplementary Fig.3D,H-I). Thus, mTORC2 signaling presents a direct mechanism whereby *Pten* homozygous deletion can promote tumor onset/progression relative to *Pik3ca* H1047R oncogenic mutation in this setting.

***Pik3ca* H1047R mutation causes p110α-dependent prostate cancer.** Recent reports have demonstrated that p110α and p110β isoforms of the PI3K catalytic subunit play distinct cellular functions and are regulated independently by differential binding partners(22-25). For instance, *in vitro* assays have established that Ras subfamily members can directly bind to the Ras binding domain (RBD) of p110α (and not p110β) to activate p110α kinase activity, and p110β RBD:RAC1 interactions have been shown to be required for GPCR-mediated p110β signaling(22-24). Moreover, *Pten*-deleted prostate cancers are considered to preferentially activate the p110β isoform, and p110β blockade has been shown to activate p110α owing to relief of feedback inhibition (e.g. via IGF1R)(25-28). Thus, we sought to determine if the phenotypic difference between *Pten* loss and *Pik3ca* oncogenic mutation reflects differential activation of PI3K catalytic isoforms. To this end, we performed IHC to detect p-ERK, a downstream target of the RAS cascade, and activation of RAC1 GTPase in *Pik3ca*$^{+/HR}$ and

Pten$^{fl/fl}$ prostate tumors to distinguish activation of RAS-p110α and RAC1-p110β signaling axes respectively. We find that p-ERK expression is markedly elevated in *Pik3ca*$^{+/HR}$ and *Pten*$^{fl/fl}$ prostate tumors compared to age-matched *Wt* controls, indicating p110α signaling is activated in both models (Fig.4A). However, only *Pten*$^{fl/fl}$ prostate tumors displayed Active-RAC-1 GTP staining (Fig.4B), indicating that activation of p110β signaling may promote prostate cancer growth induced by *Pten*-deletion.

To directly test p110α and p110β isoform dependency in *Pik3ca* mutant and *Pten* deleted prostate cancers, we administered isoform specific inhibitors (A66, a p110α-specific inhibitor or TGX-221, a p110β-specific inhibitor) or a pan-PI3K inhibitor (BKM120) to cohorts of *Pik3ca*$^{+/HR}$ and *Pten*$^{fl/fl}$ mice with prostate carcinoma for 4 weeks. *Pik3ca*$^{+/HR}$ tumor burden regressed significantly in response to A66 and BKM120 while TGX-221 had no effect, indicative of p110α-dependency (Fig.4C). In contrast, *Pten*$^{fl/fl}$ tumor burden was not reduced upon single isoform specific inhibitor treatment but did respond to BKM120 or combined A66 and TGX-221 therapy, suggesting *Pten*-deleted tumors are p110β/p110α co-dependent (Fig.4D). Histopathological analysis of prostate lobes confirmed tumor regression in A66 and BKM120 treated *Pik3ca*$^{+/HR}$ mice, and BKM120 treated *Pten*$^{fl/fl}$ mice (Fig.4E, Supplementary Fig.4A-C). These data suggest that p110β–mediated signaling events could facilitate *Pten*-deleted prostate cancer but not *Pik3ca* H1047R mutated prostate cancer, and support previous work showing that combined p110α and p110β blockade improves therapeutic outcome in *PTEN*-deficient prostate cancers compared to PI3K isoform specific monotherapy(22,26,28). Indeed, PI3K pathway inhibitors on their own have been shown to have limited efficacy in the clinic due to multiple feedback loops, PI3K-independent pathways and/or additional oncogenic mutations, and can cause side effects (e.g. hyperglycemia)(22,26,28,29). Thus, treatment

approaches that combine PI3K pathway inhibitors with other therapeutic agents are currently being explored to improve prostate cancer patient outcome."

***Pten*-deletion and *Pik3ca*$^{+/HR}$ mutation cooperate to accelerate prostate cancer progression in mice.** Given that we have found that *PIK3CA* mutation and *PTEN* loss are not mutually exclusive events in prostate cancer patients, we sought to generate a new clinically relevant model of prostate cancer, and to test if PI3K genetic drivers can cooperate to facilitate prostate cancer growth. Hence, we crossed *Pik3ca*$^{+/HR}$ mutants with *Pten*$^{fl/fl}$ animals to develop *PBiCre*$^{+/-}$*;Pik3ca*$^{+/HR}$*;Pten*$^{fl/fl}$ compound mutants (termed *Pik3ca*$^{+/HR}$*;Pten*$^{fl/fl}$) that harbour *Pik3ca*$^{+/HR}$ mutation and bi-allelic *Pten* loss in prostate epithelial cells. At 56 and 100 d we observed aggressive, locally invasive carcinoma with 100% incidence in all *Pik3ca*$^{+/HR}$*;Pten*$^{fl/fl}$ prostate lobes (Fig.5A-B, Supplementary Fig.5A-B, Supplementary Table 5). IHC analysis revealed that *Pik3ca*$^{+/HR}$*;Pten*$^{fl/fl}$ prostate tumors resemble *Pten*$^{fl/fl}$ tumors, where the CK5+ basal cell population is expanded/mislocalized and the CK8+ luminal cells are predominant (Supplementary Fig.5C). Local invasion was confirmed by the absence of SMA staining (Supplementary Fig.5C). Tumor burden was also significantly greater in compound mutants than age-matched single mutants (Supplementary Fig.5D). Visceral metastases were not detected by 100 d of age, and the development of non-prostate malignancies reflecting leaky *PBiCre*-mediated recombination (predominantly benign buccal mucosal/cutaneous papillomas and penile prolapse) prevented further ageing of *Pik3ca*$^{+/HR}$*;Pten*$^{fl/fl}$ mice.

To investigate the mechanism underpinning cooperation between *Pik3ca* mutation and *Pten* loss, we determined the number of proliferative and apoptotic cells in *Pik3ca*$^{+/HR}$*, Pten*$^{fl/fl}$ and *Pik3ca*$^{+/HR}$*;Pten*$^{fl/fl}$ locally invasive prostate carcinomas by PCNA and CC3 IHC respectively. We show that compound mutant tumors have significantly more PCNA-positive proliferating

cells than single mutants (Fig.5C-D), while CC3-mediated apoptosis is unaltered (Supplementary Fig.5E-F). These findings indicate that *Pik3ca* oncogenic mutation and *Pten* loss synergize to accelerate prostate cancer progression by increasing proliferation, but not survival.

To ascertain if the increased proliferation in $Pik3ca^{+/HR};Pten^{fl/fl}$ mice reflects further activation of mTORC1/2 signaling, we performed IHC to detect p-AKT Thr308 that leads to mTORC1 activation, as well as the phosphorylation of known mTORC1/2 downstream signaling targets. Quantitation of IHC staining revealed that the number of cells expressing membranous p-AKT Thr308 is significantly increased in $Pik3ca^{+/HR};Pten^{fl/fl}$ prostate carcinomas compared to stage-matched single mutants (Fig.5E and Supplementary Fig.5G). In accordance, mTORC1 downstream targets, p-RPS6 and p-4E-BP1 positively correlated with p-AKT Thr308 activation (Fig.5F-G, Supplementary Fig.5G), indicating increased mTORC1 signaling accelerates prostate cancer growth in $Pik3ca^{+/HR};Pten^{fl/fl}$ mutants. Phosphorylation of mTORC2 downstream targets p-AKT Ser473 and p-NDRG1 was also significantly increased in compound mutants compared to single mutants (Fig.5H-I, Supplementary Fig.5G). Taken together, these findings suggest that further potentiation of mTORC1 and mTORC2 signaling, which correlates with super-activation of AKT at Thr308/Ser473, contributes to the cooperative relationship between *Pik3ca* mutation and *Pten* loss during prostate cancer in this setting.

Previous work has shown that amplification/overexpression of *Pik3ca* and *Pik3cb* increases oncogenicity(22,30,31), and amplification frequently correlates with poor patient outcome in multiple malignancies(22). To establish if *Pik3ca/b* transcripts are expressed at physiological levels in $Pik3ca^{+/HR}$, $Pten^{fl/fl}$ and $Pik3ca^{+/HR};Pten^{fl/fl}$ prostate carcinomas, we performed RNA

in situ hybridisation, and quantitated RNA molecules relative to *Wt* controls. We show that *Pik3ca* and *Pik3cb* mRNA is significantly increased in double mutant prostate tumors compared to $Pten^{fl/fl}$ and $Pik3ca^{+/HR}$ single mutant tumors, and age-matched *Wt* controls (Fig.5J-L, Supplementary Fig.5H). However, the functional consequence(s) of *Pik3ca* and *Pik3cb* mRNA upregulation remain elusive.

***Pik3ca*$^{+/HR}$ and *Pten*$^{fl/fl}$ induced prostate cancers acquire CRPC in mice.** PTEN loss is widely reported to correlate with resistance to androgen deprivation therapy in prostate cancer patients and mice(9,32,33). To examine if $Pik3ca^{+/HR}$-driven prostate cancer also confers castration resistant disease, we aged cohorts of $Pik3ca^{+/HR}$ mutant mice until invasive prostate carcinoma had developed (300 d) and assessed the early and long-term response to surgical castration. Although we observed a significant reduction in $Pik3ca^{+/HR}$ total prostate weight at 2 and 10 weeks post-castration (Fig.6A), histopathological analysis revealed that prostate tumors were still present in $Pik3ca^{+/HR}$ mice, indicating the development of acquired CRPC (Fig.6B, Supplementary Fig.6A). These findings are in keeping with partial androgen sensitivity and the latent acquisition of CRPC, mirroring homozygous deletion of *Pten* (Fig.6A and B, Supplementary Fig.6A), as previously reported(33,34). IHC to detect AR confirmed the reduction of androgens post-castration, as cytoplasmic AR was detected in $Pik3ca^{+/HR}$ and $Pten^{fl/fl}$ prostate epithelial cells following castration, whereas uncastrated controls displayed active nuclear AR (Supplementary Fig.6B).

To determine if *Pik3ca* heterozygous oncogenic mutation sensitises pre-neoplastic prostate epithelium to CRPC transition, we examined the short-term and long-term response of $Pik3ca^{+/HR}$ mice to castration at 100 d, when only hyperplastic disease is present. Prostate epithelial regression was detected 2 weeks post-castration and correlated with a reduction in

prostate weight, yet small prostate hyperplastic and dysplastic tumors, resembling uncastrated *Pik3ca*$^{+/HR}$ mutants, had developed by 42 weeks post-castration in 100% (6/6) and 67% (4/6) of cases respectively (Supplementary Fig.6C-D). These data demonstrate that *Pik3ca*-mutated prostate epithelium possesses an inherent ability to acquire CRPC, similarly to *Pten* loss(9).

***Pik3ca* oncogenic mutation and *Pten* loss synergize, predisposing to *de novo* CRPC.** Next, we castrated *Pik3ca*$^{+/HR}$;*Pten*$^{fl/fl}$ mice at 100 d of age when invasive carcinoma was present, to test if *Pik3ca* mutation and *Pten* loss can also cooperate to promote CRPC growth. At 2 weeks post-castration, castrated compound mutants phenocopied intact controls, and no appreciable difference in tumor burden was detected (Fig.6C-D). These findings contrast the partial regression observed in the single mutants and indicate that *Pik3ca* oncogenic mutation and *Pten* homozygous deletion cooperate to promote *de novo* CRPC *in vivo*. In support, single mutants displayed a significant reduction in the percentage of PCNA-positive proliferative cells and elevated CC3-positive apoptotic cells 2 weeks post-castration, which were unaltered in compound mutants (Fig.6E-F, Supplementary Fig.7A-B). These data indicate that *de novo* CRPC in *Pik3ca*$^{+/HR}$;*Pten*$^{fl/fl}$ mice is attributable to both the sustained level of proliferation and castration-induced apoptosis evasion. In accordance with *de novo* CRPC, IHC to detect AR also revealed that a noticeable proportion of *Pik3ca*$^{+/HR}$;*Pten*$^{fl/fl}$ prostate epithelial cells displayed AR activation (i.e. nuclear translocation) 2 weeks post-castration, which were not apparent in single mutants at this early time point (Supplementary Fig.6B). Of note, *Nkx3.1* and *Pbsn*, AR transcriptional target genes, are significantly reduced in *Pik3ca*$^{+/HR}$ prostate carcinomas relative to *Wt* prostate, and levels were further diminished in *Pten*$^{fl/fl}$ and *Pik3ca*$^{+/HR}$;*Pten*$^{fl/fl}$ tumors (Supplementary Fig.7C-D). These findings support previous work indicating that PI3K activation perturbs AR-mediated signaling(29), and indicate that *Pbsn* and *Nkx3.1* transcription is not likely to facilitate *de novo* CRPC in this setting.

The molecular mechanisms underpinning the emergence of CRPC are largely unknown. *Pten*-deleted CRPC acquisition has been previously associated with elevated AKT signaling, suggesting that further activation of the AKT cascade contributes to CRPC transition(9). In support, we observed a significant increase in the percentage of cells positive for mTORC1 signaling components p-AKT (Thr308), p-RPS6 (Ser235/236) and p-4E-BP1 (Thr37/46) and the mTORC2 target p-AKT (Ser473) in both the $Pik3ca^{+/HR}$ and $Pten^{fl/fl}$ models just 2 weeks post-castration (Fig.7A-D). Notably, phosphorylation of NDRG1 was not altered in either model post-castration (Fig.7E). Thus, *Pten*-deleted and *Pik3ca*-mutated prostate epithelial cells appear to hyperactivate AKT upon castration, which elevates mTORC1 signaling downstream targets to facilitate CRPC transition. Nevertheless, we do not exclude the possibility that additional molecular events may also contribute to CRPC transition in these models, including PTEN and/or AKT signal transduction independent of PI3K(2,35).

Our analysis of $Pik3ca^{+/HR};Pten^{fl/fl}$ prostate tumors pre- and post-castration revealed that the high proportion of p-AKT (Thr308), p-RPS6 (Ser235/236) and p-AKT (Ser473) positive cells is maintained at a super-activated state, and that the percentage of p-4E-BP1 (Thr37/46) and p-NDRG1 (Thr346) cells is increased even further (Fig.7A-E). Despite an increase in p-4E-BP1 in $Pten^{fl/fl}$ and $Pik3ca^{+/HR};Pten^{fl/fl}$ castrated tumors compared to $Pik3ca^{+/HR}$ castrated animals, p-4E-BP1 was not significantly elevated in compound mutants compared to the $Pten^{fl/fl}$ model, signifying 4E-BP1 phosphorylation at Thr37/46 and subsequent inactivation are not likely to promote *de novo* CRPC formation. However, our findings suggest that NDRG1 inactivation may contribute to *de novo* CRPC. In addition to increased phosphorylation of NDRG1 post-castration, androgen deprivation in $Pik3ca^{+/HR};Pten^{fl/fl}$ mice also positively correlated with p-NDRG1 nuclear localisation (Fig.7F). Nevertheless, the precise role of NDRG1 inactivation

during *de novo* CRPC remains to be determined and warrants further investigation. Taken together, these results infer that a high threshold of AKT-hyperactivation prior to castration, and/or NDRG1-inactivation, may prove to be useful biomarkers of intrinsic CRPC in the clinic.

To explore potential mechanisms underpinning the synergistic relationship between *Pik3ca* mutation and *Pten*-deletion, and during castration-resistant disease formation, we performed a reverse-phase protein array (RPPA) on protein lysates isolated from $Pik3ca^{+/HR}$, $Pten^{fl/fl}$ and $Pik3ca^{+/HR}$; $Pten^{fl/fl}$ stage-matched uncastrated prostate carcinomas, and 2-weeks post-castration (Fig.7G, Supplementary Tables 6/7). RPPA data analysis revealed that *Pik3ca*-mutated and *Pten*-deleted prostate tumors display distinct RPPA profiles, supporting the contention that *Pik3ca* oncogenic mutation and *Pten* loss may mediate distinct signaling events to facilitate prostate cancer growth. For instance, compared to $Pik3ca^{+/HR}$ tumors, $Pten^{fl/fl}$ tumors displayed enhanced signal intensities for PI3K cascade phosphoproteins (e.g. p-AKT Thr308, p-AKT Ser473, p-FOXO3A Ser318/321, p-GSK-3β Ser9 and p-NDRG1 Thr346), whereas tyrosine kinase-mediated (p-EGFR Tyr1173, p-SHP-2 Tyr542, p-SRC family Tyr416) and MAPK (p-ERK1/2 Thr202/Tyr204) phosphoproteins were elevated in $Pik3ca^{+/HR}$ tumors (Fig.7G and Supplementary Table 7). Interestingly, $Pik3ca^{+/HR}$ and $Pten^{fl/fl}$ prostate carcinomas did not display significant differences in RPPA signal intensities for the senescence markers p21 or p27 (Fig. 7G, Supplementary Table 7), suggesting that the observed phenotypic differences are not due to changes in senescence. A significant increase in p53 signal intensity was observed in $Pten^{fl/fl}$ tumors relative to $Pik3ca^{+/HR}$ tumors. As p21 and p27 are unaltered, these findings indicate that the observed changes in p53 are not regulating senescence, but may instead be mediating other cellular functions, such as apoptosis. This correlates with our observations in CC3 and phosphorylated p53 (Ser15) (Fig.7G, Supplementary Fig.3B,

Supplementary Table 7). RPPA results for p-AKT Thr308 and p-AKT Ser473 were confirmed by Western blotting (Supplementary Fig.7E).

RPPA profiles for uncastrated and castrated compound mutants were strikingly similar. Indeed, only 4 targets were significantly altered; p-SHP-2 (Tyr542) and p-SRC family (Tyr416) signals were increased and YAP and CK2α were decreased (Fig.7G, Supplementary Table 7). This result contrasts single mutants that acquired CRPC and is consistent with the general lack of effect of castration on the prostate tumors in the double mutant mice (Fig.6C-F). However, it should be noted that the RPPA was not sensitive enough to detect elevated p-NDRG1 (Thr346) in $Pik3ca^{+/HR}$;$Pten^{fl/fl}$ mutants post-castration that was observed by IHC (Fig.7E-F), presumably owing to tumor heterogeneity and/or stromal content, which may also be a contributing factor in the lack of significant difference in other proteins as well. Nevertheless, distinct differences between the $Pik3ca^{+/HR}$ and $Pten^{fl/fl}$ models were detected post-castration (Fig.7G, Supplementary Table 7). For instance, *Pik3ca*-mutated tumors displayed a significant increase in IGF1Rβ and p-NF-kB p65 (Ser 536) signal intensities post-castration, which were not altered in *Pten*-deleted tumors post-castration. Additionally, castrated $Pik3ca^{+/HR}$ tumors displayed elevated JAK/STAT and MAPK signaling relative to castrated $Pten^{fl/fl}$ tumors. Taken together, our findings suggest that *Pik3ca* oncogenic mutation and *Pten* loss may mediate distinct signaling events to facilitate prostate cancer growth and resistance to castration.

Discussion

We report that *PIK3CA* mutation/amplification positively correlates with poor prostate cancer patient prognosis and overall survival. Our findings are the first to demonstrate that the *PIK3CA* H1047R oncogenic mutation is sufficient to cause invasive prostate cancer *in vivo* and that

concomitant loss of *PTEN* and *PIK3CA* mutation, which frequently occurs in the clinic, can cooperate to accelerate prostate cancer growth in mice.

Our data support the hypothesis that different genetic drivers of the PI3K cascade are not functionally redundant, but instead drive prostate tumorigenesis via distinct signaling events. We show that relative to p110α-dependent *Pik3ca*$^{+/HR}$-induced prostate cancers, *Pten*$^{fl/fl}$ prostate tumors are p110α/β co-dependent, and exhibit accelerated tumor formation and progression owing to AKT-hyperactivation, elevated mTORC2 and RAC1-p110β signaling. The failure to induce robust AKT signaling in *Pik3ca*$^{+/HR}$ epithelium is probably attributable to the maintenance of PTEN tumor suppressive function that reduces PIP_3 levels, AKT membrane recruitment, and subsequent activation of AKT, as previously reported(35). In corroboration, *Pten* loss has been shown to positively correlate with disease progression in mice, as *Pten* loss of heterozygosity is required for prostate cancer growth in *Pten* heterozygous prostate epithelium(9). We speculate that PTEN function is also likely to be conserved in transgenic mice expressing myristoylated/activated AKT or p110β in prostate epithelial cells, as only low-grade prostate epithelial neoplasia develops that does not progress to carcinoma with ageing(36,37). Taken together, these observations suggest that additional mTORC2/RAC1/p110β-independent cooperative events are likely to facilitate malignant progression to an invasive state in *Pik3ca*$^{+/HR}$ mutants that express PTEN. Indeed, *PIK3CA* mutations have been shown to potentiate a PDK1-SGK3, AKT-independent signaling axis in various human cancer cell lines that express PTEN(35), and PDK1-SGK1 AKT-independent signaling has been shown to cause resistance to p110α inhibition by directly phosphorylating TSC2 to activate the mTORC1 pathway(38).

Guertin and colleagues have previously shown that *RICTOR*, a key regulatory component of mTORC2, is required for PC3 *PTEN*-null human prostate cancer cells to form tumor xenografts, and that bi-allelic deletion of *Rictor* prevents prostate cancer formation driven by *Pten* loss in mice by reducing proliferation and AKT phosphorylation at Ser473(39). We show that $Pten^{fl/fl}$ mice displayed early prostate tumor formation and accelerated progression relative to $Pik3ca^{+/HR}$ mutants, reflecting elevated mTORC2 signalling and subsequent AKT phosphorylation at Ser473 in the context of *Pten* loss. Thus, our findings support the notion that mTORC2 signalling plays a critical role during prostate tumorigenesis and progression, and strengthen the rationale for mTORC2-targeted therapy in *PTEN*-deleted prostate cancer.

The absence of p-AKT Ser473 phosphorylation in $Pik3ca^{+/HR}$ mutant prostate cancer may be attributable to reduced PIP_3 levels and/or distinct AKT regulation in *Pten*-null and *Pik3ca* mutant prostate cancers, as AKT phosphorylation is dependent on a plethora of AKT protein kinases and phosphatases(5). Of note, the mechanism of AKT regulation may also depend upon the type of *PIK3CA* mutation (i.e. helical vs kinase) and tissue context, as several human cancer cell lines with *PIK3CA* kinase mutations have been shown to express high levels of p-AKT Ser473 and Thr308 in the presence of PTEN(35). PTEN is also reported to play a broader AKT-independent tumor suppressive role via protein- and lipid-phosphatase activities to mediate p53, cell cycle arrest and integrin, insulin and focal adhesion kinase signaling, reviewed in(40). Thus, developing our combined understanding of AKT regulation, p110 PI3K isoform signaling, and PTEN mode of action during prostate cancer is vital to determine optimal therapeutic approaches that inhibit the PI3K signaling network and subsequently prostate cancer growth and progression.

Although p110α and p110β isoforms have been shown to form mutually exclusive signaling complexes with RAS and RHO family (RAC1/CDC42) small GTPase protein superfamily members respectively(22), the molecular mechanisms underpinning their different modes of action are poorly understood. This study provides additional data that underlines a distinct role for the RAC1-p110β signaling axis in *Pten*-deleted prostate cancer, and raises the possibility that RAC inhibition may show therapeutic efficacy against *PTEN*-deleted prostate cancer in the clinic, as recently demonstrated for a *Pten*-null, p110β-dependent mouse model of myeloid neoplasia(41). By taking this approach, PI3K-independent functions of PTEN and AKT may be advantageously co-targeted, as RAC1 activation is mediated by PI3K-dependent (e.g. PREX-1/TIAM/mTORC2) and PI3K-independent (e.g. SRC/p130CAS) signaling(25,42).

We have generated a new clinically relevant transgenic mouse model of advanced prostate cancer driven by concomitant *Pik3ca* heterozygous oncogenic mutation and *Pten* homozygous deletion. We show that these two oncogenic drivers cooperate to promote rapid progression to invasive prostate cancer, characterised by the synergistic elevation of mTORC1/2 signaling, AKT super-activation and increased *Pik3ca/b* mRNA transcript expression. These data provide direct evidence that *Pik3ca* mutation and *Pten* deletion coordinate independent oncogenic signaling events during prostate cancer, in corroboration with the distinct RPPA profiles observed. Furthermore, our findings emphasize that the co-existence of mutated *PIK3CA* and *PTEN* loss may prove to be an important prognostic indicator for rapid prostate cancer progression and *de novo* resistance to androgen deprivation therapy in the clinic.

Currently, the cause and consequence of upregulated *Pik3ca/b* transcription is poorly understood. Theoretically, increased *Pik3ca/b* gene expression could promote prostate cancer progression in $Pik3ca^{+/HR};Pten^{fl/fl}$ mice by increasing p110α/β protein levels, and thus total

PI3K activity, as *PIK3CA* amplification is thought to do in ovarian cancer cells (43). FOXO3A, NF-kB, YB1 and p53 have been shown to promote *PIK3CA* transcription (reviewed in(44)), however *PIK3CB* transcriptional regulators remain to be identified. Further investigation is needed to determine the underlying mechanism by which increased p110 catalytic activity and loss of Pten phosphatase activity cooperate to upregulate *Pik3ca* and *Pik3cb* transcription, and to establish the functional significance of this observation.

Despite numerous phenotypic differences, we report that both *Pten*-null and *Pik3ca*$^{+/HR}$-driven prostate cancers are partially sensitive to androgen withdrawal and acquire CRPC in association with augmented PI3K signaling. These data signify that both p110α and p110β PI3K catalytic isoforms can induce PI3K signaling in response to androgen deprivation, supporting previous *in vitro* work in the PTEN-deficient human prostate cancer LNCaP cell line that showed PI3K signaling induced by an AR-inhibitor is diminished by p110α or p110β inhibition(26). Since, AKT-hyperactivation and augmented mTORC1/2 are consistent features of intact *Pik3ca*$^{+/HR}$;*Pten*$^{fl/fl}$ prostate tumors, it is tempting to speculate that AKT-hyperactivation may be a pre-requisite for *de novo* CRPC in this setting. In addition, innate CRPC in *Pik3ca*$^{+/HR}$;*Pten*$^{fl/fl}$ compound mutants was associated with increased phosphorylation of the mTORC2-SGK substrate NDRG1 at Thr346, suggesting that NDRG1 inactivation may facilitate *de novo* CRPC. Significantly, NDRG1 has been shown to function as a metastasis suppressor in mouse xenograft models of prostate cancer by reducing Activating Transcription Factor 3 (*ATF3*) transcription, and *NDRG1* mRNA down-regulation correlates with Gleason score and worse prostate cancer survival(45). Stein and colleagues have also reported that NDRG1 is a p53 transcriptional target that is required for p53-mediated apoptosis(46). Given that *Pik3ca*$^{+/HR}$;*Pten*$^{fl/fl}$ prostate tumors evade castration-induced apoptosis and proliferation arrest, it will be important for future studies to determine if NDRG1 inactivation contributes to

CRPC transition. However, since oncogenic PI3K/AKT signaling has been linked to increased genomic instability(47), we do not exclude the possibility that *Pik3ca*$^{+/HR}$;*Pten*$^{fl/fl}$ prostate tumors create an environment capable of inducing additional oncogenic mutations that promote CRPC formation.

It is becoming clear that approaches inhibiting multiple targets within the PI3K network, either simultaneously or sequentially, are necessary to enhance therapeutic efficacy. Thus, further characterization of p110α/β-mediated signaling, PI3K-independent PTEN tumor suppressive functions, AKT-independent signaling and AKT regulation is required to improve our understanding of how to target the PI3K network and identify mechanisms of therapeutic resistance to improve our management of prostate cancer in the clinic. Future work addressing how to personalise treatment for tumors driven by diverse PI3K genetic drivers is paramount, and is likely to entail the co-inhibition of PI3K-dependent and PI3K/AKT-independent signaling pathways.

Materials and Methods

Experimental animals: PBiCre transgenic mice that express *Cre* recombinase under the control of the *Probasin* promoter and *Pten*$^{fl/fl}$ mice have been described previously(21,48). *Pik3ca*^{H1047R} mutant mice were generated in-house(11). All mice were maintained on a pure FVB/NJ background. Mice were genotyped from DNA isolated from toe biopsies, as described previously(11,49). Age-matched males were randomly assigned to uncastrated/castrated cohorts. Castration experiments involved the surgical removal of the testis and epididymis. Animal experiments followed the National Health and Medical Research Council (NHMRC) Australian Code of Practice for the Care and Use of Animals for Scientific Purposes and were

approved by the Animal Experimentation Ethics Committee at Peter MacCallum Cancer Centre.

Tissue isolation and histology: Tissue was harvested and fixed for 16-24 h in 10% neutral-buffered formaldehyde at 4°C before being paraffin embedded and sectioned at 4 μm. Sections were stained with haematoxylin/eosin for histological analysis by a certified pathologist (P.W.) blinded to genotype/treatment. Defining characteristics for prostate disease were based upon the pathological classification of mouse prostate disease outlined in (50).

Immunohistochemistry: Staining was carried out as described previously(49) on formalin-fixed, paraffin-embedded (FFPE) sections. Primary antibodies: Active RAC1-GTP 1:800 (#26903, NewEast Biosciences), AR 1:300 (#sc-816, Santa Cruz), PCNA 1:400 (#610665, BD Biosciences Pharmingen), and Cell Signalling Technology antibodies: Cleaved Caspase-3 1:300 (#9664), p-AKT (Ser473) 1:400 (#4060), p-AKT (Thr308) 1:400 (#13038), p-ERK (Thr202/Tyr204) 1:200 (#4376), PTEN 1:300 (#9559), p-RPS6 (Ser235/236) 1:400 (#2211), p-NDRG1 (Thr346) 1:800 (#5482) and p-4E-BP1 (Thr37/46) 1:200 (#2855). IHC scoring represents the mean percentage of positive cells counted from 8-10 images/mouse (200x magnification, BX-51 Olympus microscope, n=3/genotype).

PI3K inhibitor administration: Cohorts of male *Pik3ca*$^{+/HR}$ or *Pten*$^{fl/fl}$ mice were treated at 400 and 200 d old respectively: A66 (p110α-specific inhibitor, 100 mg/kg, daily p.o.), TGX-221 (p110β-specific inhibitor, 30 mg/kg, daily p.o.) and BKM120 (pan-PI3K inhibitor, 40 mg/kg, daily p.o.). Inhibitors were dissolved in filter-sterilised 20% hydroxyproyl-beta-cyclodextrin (Sigma), sonicated for 10 minutes and dosed immediately (4 weeks; 5 d on, 2 d off). No appreciable toxicity was observed (i.e. >20% weight loss). A66 and TGX-221 were generated

in house by P.R.S. (University of Auckland, New Zealand) and BKM120 was obtained from SYNkinase (Australia).

RNA in situ hybridisation: FFPE mouse prostate tissue sections were probed using the RNAscope® 2.5 high-definition red detection kit (#322350, Advanced Cell Diagnostics). Slides were counterstained with hematoxylin. Scoring represents the average number of RNA molecules per 50 cells/mouse (400x magnification, BX-43 Olympus microscope, n=3/genotype).

RPPA: Protein lysates were prepared from snap frozen tissue homogenized in CLB1 buffer (Zeptosens, Bayer), and quantified using a Pierce™ Coomassie Plus (Bradford) Protein Assay Kit (n=3/cohort). Using a Sciclone/Caliper ALH3000 liquid handling robot (Perkin Elmer), samples were serially diluted in 10% CLB1:90% CSBL1 buffer (Zeptosens, Bayer) and spotted onto ZeptoChips (Zeptosens) in duplicate using a Nano-plotter-NP2.1 non-contact microarray system (GeSim). Chips were blocked under non-contact conditions for 1 hour with BB1 buffer (Zeptosens), incubated with pre-validated primary antibodies (1:500, 20 hours), and Alexa Fluor® 647 anti-rabbit secondary antibody (1:1000, 4 hours) (#Z-25308, Thermo Fisher Scientific). Chips were read on a Zeptosens instrument and software version 3.1 used to calculate the relative fluorescence intensity. All samples were normalised to the background values reported in the secondary antibody-only negative control. Pearson's correlation was calculated to confirm replicate pairs were adequately correlated (correlation coefficient >0.9). Data were Log2-normalised, median centered and re-scaled between 0-1 using the formula; $\frac{ab-\min(ab)}{\max(ab)-\min(ab)}$. ab represents a vector of antibody responses for a given sample. The RPPA heatmap was generated in R using pheatmap.

Analysis of genomic datasets: Analysis of *PIK3CA* gene mutation/amplification was performed on prostate cancer patient datasets with sequencing and copy number alteration (CNA) data using the cBioPortal platform(14). The TCGA provisional dataset was downloaded from the TCGA data portal (https://tcga-data.nci.nih.gov/); *PIK3CA* segment mean Log R-Ratio ≥0.135. To minimise CNA noise, probe number was filtered to ≤10. Silent mutations were excluded.

Statistical analysis: Prostate weight and IHC scoring were analysed using a one-way ANOVA with Tukey's correction or an unpaired t-test (95% confidence interval) as indicated using GraphPad Prism_7.03 software. Kaplan-Meier plots were generated, and age-adjusted COX proportional hazard regression ratio calculated using R software. For RPPA, an unpaired two-tailed t-test with Welch's correction was calculated using R software. $P<0.05$ was considered statistically significant.

References

1. Ferlay J, Soerjomataram I, Dikshit R, Eser S, Mathers C, Rebelo M, *et al.* Cancer incidence and mortality worldwide: sources, methods and major patterns in GLOBOCAN 2012. International journal of cancer **2015**;136:E359-86.
2. Vanhaesebroeck B, Stephens L, Hawkins P. PI3K signalling: the path to discovery and understanding. Nature reviews Molecular cell biology **2012**;13:195-203.
3. Martini M, De Santis MC, Braccini L, Gulluni F, Hirsch E. PI3K/AKT signaling pathway and cancer: an updated review. Annals of Medicine **2014**;46:372-83.
4. Lemmon MA. Membrane recognition by phospholipid-binding domains. Nature reviews Molecular cell biology **2008**;9:99-111.
5. Chan CH, Jo U, Kohrman A, Rezaeian AH, Chou PC, Logothetis C, *et al.* Posttranslational regulation of Akt in human cancer. Cell & bioscience **2014**;4:59.

6. Garcia-Martinez JM, Alessi DR. mTOR complex 2 (mTORC2) controls hydrophobic motif phosphorylation and activation of serum- and glucocorticoid-induced protein kinase 1 (SGK1). The Biochemical journal **2008**;416:375-85.

7. Grasso CS, Wu YM, Robinson DR, Cao X, Dhanasekaran SM, Khan AP, *et al.* The mutational landscape of lethal castration-resistant prostate cancer. Nature **2012**;487:239-43.

8. Taylor BS, Schultz N, Hieronymus H, Gopalan A, Xiao Y, Carver BS, *et al.* Integrative genomic profiling of human prostate cancer. Cancer cell **2010**;18:11-22.

9. Mulholland DJ, Tran LM, Li Y, Cai H, Morim A, Wang S, *et al.* Cell autonomous role of PTEN in regulating castration-resistant prostate cancer growth. Cancer cell **2011**;19:792-804.

10. Karakas B, Bachman KE, Park BH. Mutation of the PIK3CA oncogene in human cancers. British journal of cancer **2006**;94:455-9.

11. Kinross KM, Montgomery KG, Kleinschmidt M, Waring P, Ivetac I, Tikoo A, *et al.* An activating Pik3ca mutation coupled with Pten loss is sufficient to initiate ovarian tumorigenesis in mice. J Clin Invest **2012**;122:553-7.

12. Rudd ML, Price JC, Fogoros S, Godwin AK, Sgroi DC, Merino MJ, *et al.* A unique spectrum of somatic PIK3CA (p110α) mutations within primary endometrial carcinomas. Clinical cancer research **2011**;17:1331-40.

13. Forbes SA, Beare D, Gunasekaran P, Leung K, Bindal N, Boutselakis H, *et al.* COSMIC: exploring the world's knowledge of somatic mutations in human cancer. Nucleic acids research **2015**;43:D805-11.

14. Gao J, Aksoy BA, Dogrusoz U, Dresdner G, Gross B, Sumer SO, *et al.* Integrative analysis of complex cancer genomics and clinical profiles using the cBioPortal. Science signaling **2013**;6:pl1.

15. Dogruluk T, Tsang YH, Espitia M, Chen F, Chen T, Chong Z*, et al.* Identification of Variant-Specific Functions of PIK3CA by Rapid Phenotyping of Rare Mutations. Cancer research **2015**;75:5341-54.

16. Gymnopoulos M, Elsliger M-A, Vogt PK. Rare cancer-specific mutations in PIK3CA show gain of function. Proceedings of the National Academy of Sciences **2007**;104:5569-74.

17. Abeshouse A, Ahn J, Akbani R, Ally A, Amin S, Andry Christopher D*, et al.* The Molecular Taxonomy of Primary Prostate Cancer. Cell;163:1011-25.

18. Lin DI. Improved survival associated with somatic PIK3CA mutations in copy-number low endometrioid endometrial adenocarcinoma. Oncology letters **2015**;10:2743-8.

19. Yuan TL, Cantley LC. PI3K pathway alterations in cancer: variations on a theme. Oncogene **2008**;27:5497-510.

20. Oda K, Stokoe D, Taketani Y, McCormick F. High frequency of coexistent mutations of PIK3CA and PTEN genes in endometrial carcinoma. Cancer research **2005**;65:10669-73.

21. Jin C, McKeehan K, Wang F. Transgenic mouse with high Cre recombinase activity in all prostate lobes, seminal vesicle, and ductus deferens. The Prostate **2003**;57:160-4.

22. Thorpe LM, Yuzugullu H, Zhao JJ. PI3K in cancer: divergent roles of isoforms, modes of activation and therapeutic targeting. Nature reviews Cancer **2015**;15:7-24.

23. Rodriguez-Viciana P, Warne PH, Vanhaesebroeck B, Waterfield MD, Downward J. Activation of phosphoinositide 3-kinase by interaction with Ras and by point mutation. The EMBO journal **1996**;15:2442-51.

24. Fritsch R, de Krijger I, Fritsch K, George R, Reason B, Kumar MS*, et al.* RAS and RHO families of GTPases directly regulate distinct phosphoinositide 3-kinase isoforms. Cell **2013**;153:1050-63.

25. Zhang J, Gao X, Schmit F, Adelmant G, Eck MJ, Marto JA*, et al.* CRKL Mediates p110β-Dependent PI3K Signaling in PTEN-Deficient Cancer Cells. Cell Reports **2017**;20:549-57.

26. Schwartz S, Wongvipat J, Trigwell CB, Hancox U, Carver BS, Rodrik-Outmezguine V*, et al.* Feedback suppression of PI3Kalpha signaling in PTEN-mutated tumors is relieved by selective inhibition of PI3Kbeta. Cancer Cell **2015**;27:109-22.

27. Wee S, Wiederschain D, Maira S-M, Loo A, Miller C, deBeaumont R*, et al.* PTEN-deficient cancers depend on PIK3CB. Proceedings of the National Academy of Sciences **2008**;105:13057-62.

28. Jia S, Gao X, Lee SH, Maira SM, Wu X, Stack EC*, et al.* Opposing effects of androgen deprivation and targeted therapy on prostate cancer prevention. Cancer Discov **2013**;3:44-51.

29. Carver BS, Chapinski C, Wongvipat J, Hieronymus H, Chen Y, Chandarlapaty S*, et al.* Reciprocal feedback regulation of PI3K and androgen receptor signaling in PTEN-deficient prostate cancer. Cancer Cell **2011**;19:575-86.

30. Kang S, Denley A, Vanhaesebroeck B, Vogt PK. Oncogenic transformation induced by the p110beta, -gamma, and -delta isoforms of class I phosphoinositide 3-kinase. Proceedings of the National Academy of Sciences of the United States of America **2006**;103:1289-94.

31. Denley A, Kang S, Karst U, Vogt PK. Oncogenic signaling of class I PI3K isoforms. Oncogene **2008**;27:2561-74.

32. Ferraldeschi R, Nava Rodrigues D, Riisnaes R, Miranda S, Figueiredo I, Rescigno P*, et al.* PTEN protein loss and clinical outcome from castration-resistant prostate cancer treated with abiraterone acetate. European urology **2015**;67:795-802.

33. Lunardi A, Ala U, Epping MT, Salmena L, Clohessy JG, Webster KA*, et al.* A co-clinical approach identifies mechanisms and potential therapies for androgen deprivation resistance in prostate cancer. Nature genetics **2013**;45:747-55.

34. Zhang W, Zhu J, Efferson CL, Ware C, Tammam J, Angagaw M*, et al.* Inhibition of Tumor Growth Progression by Antiandrogens and mTOR Inhibitor in a Pten-Deficient Mouse Model of Prostate Cancer. Cancer research **2009**;69:7466-72.

35. Vasudevan KM, Barbie DA, Davies MA, Rabinovsky R, McNear CJ, Kim JJ*, et al.* AKT-independent signaling downstream of oncogenic PIK3CA mutations in human cancer. Cancer cell **2009**;16:21-32.

36. Lee SH, Poulogiannis G, Pyne S, Jia S, Zou L, Signoretti S*, et al.* A constitutively activated form of the p110beta isoform of PI3-kinase induces prostatic intraepithelial neoplasia in mice. Proceedings of the National Academy of Sciences of the United States of America **2010**;107:11002-7.

37. Majumder PK, Yeh JJ, George DJ, Febbo PG, Kum J, Xue Q*, et al.* Prostate intraepithelial neoplasia induced by prostate restricted Akt activation: the MPAKT model. Proceedings of the National Academy of Sciences of the United States of America **2003**;100:7841-6.

38. Castel P, Ellis H, Bago R, Toska E, Razavi P, Carmona F J*, et al.* PDK1-SGK1 Signaling Sustains AKT-Independent mTORC1 Activation and Confers Resistance to PI3Kα Inhibition. Cancer Cell **2016**;30:229-42.

39. Guertin DA, Stevens DM, Saitoh M, Kinkel S, Crosby K, Sheen J-H*, et al.* mTOR Complex 2 Is Required for the Development of Prostate Cancer Induced by Pten Loss in Mice. Cancer Cell;15:148-59.

40. Blanco-Aparicio C, Renner O, Leal JF, Carnero A. PTEN, more than the AKT pathway. Carcinogenesis **2007**;28:1379-86.

41. Yuzugullu H, Baitsch L, Von T, Steiner A, Tong H, Ni J, *et al.* A PI3K p110β–Rac signalling loop mediates Pten-loss-induced perturbation of haematopoiesis and leukaemogenesis. Nature communications **2015**;6:8501.

42. Ebi H, Costa C, Faber AC, Nishtala M, Kotani H, Juric D, *et al.* PI3K regulates MEK/ERK signaling in breast cancer via the Rac-GEF, P-Rex1. Proceedings of the National Academy of Sciences of the United States of America **2013**;110:21124-9.

43. Shayesteh L, Lu Y, Kuo W-L, Baldocchi R, Godfrey T, Collins C, *et al.* PIK3CA is implicated as an oncogene in ovarian cancer. Nature genetics **1999**;21:99-102.

44. Thakur B, Ray P. p53 Loses grip on PIK3CA expression leading to enhanced cell survival during platinum resistance. Molecular oncology **2016**;10:1283-95.

45. Bandyopadhyay S, Wang Y, Zhan R, Pai SK, Watabe M, Iiizumi M, *et al.* The tumor metastasis suppressor gene Drg-1 down-regulates the expression of activating transcription factor 3 in prostate cancer. Cancer research **2006**;66:11983-90.

46. Stein S, Thomas EK, Herzog B, Westfall MD, Rocheleau JV, Jackson RS, *et al.* NDRG1 Is Necessary for p53-dependent Apoptosis. Journal of Biological Chemistry **2004**;279:48930-40.

47. Xu N, Lao Y, Zhang Y, Gillespie DA. Akt: A Double-Edged Sword in Cell Proliferation and Genome Stability. Journal of Oncology **2012**;2012:951724.

48. Lesche R, Groszer M, Gao J, Wang Y, Messing A, Sun H, *et al.* Cre/loxP-mediated inactivation of the murine Pten tumor suppressor gene. Genesis **2002**;32:148-9.

49. Pearson HB, Perez-Mancera PA, Dow LE, Ryan A, Tennstedt P, Bogani D, *et al.* SCRIB expression is deregulated in human prostate cancer, and its deficiency in mice promotes prostate neoplasia. J Clin Invest **2011**;121:4257-67.

50. Shappell SB, Thomas GV, Roberts RL, Herbert R, Ittmann MM, Rubin MA, *et al.* Prostate pathology of genetically engineered mice: definitions and classification. The

consensus report from the Bar Harbor meeting of the Mouse Models of Human Cancer Consortium Prostate Pathology Committee. Cancer research **2004**;64:2270-305.

Author's contributions:

Conception and design: H.B. Pearson, O.J. Sansom and W.A. Phillips

Development of methodology: H.B. Pearson, J. Li, C. Cullinane, P. Waring, L. Furic, K. Koushyar, T.J. Phesse, O.J. Sansom and W.A. Phillips.

Acquisition of data: H.B. Pearson, J. Li, V.S. Meniel, C.M. Fennell, P. Waring, K.G. Montgomery, R.J. Rebello, A.A MacPherson, S. Koushyar, K.J. Simpson, L. Furic, C. Cullinane, T.J. Phesse, P.R. Shepherd and O.J. Sansom.

Analysis and interpretation of data: H.B. Pearson, J. Li, P. Waring, T.J. Phesse, O.J. Sansom and W.A. Phillips.

Writing, review and/or revision of the manuscript: H.B. Pearson and W.A. Phillips wrote and revised the manuscript, all authors reviewed it.

Administrative, technical, or material support: H.B. Pearson, J. Li, K.J. Simpson, P.O. Humbert and P.R. Shepherd.

Study supervision: H.B. Pearson and W.A. Phillips,

Acknowledgements

The authors wish to thank the animal, bioinformatics, VCFG-RPPA, microscopy and histology core facilities at the Peter MacCallum Cancer Centre for supporting this project, and the histology departments at the Beatson Institute of Cancer research and the European Cancer Stem Cell Research Centre. We also thank Nathan Crouch (VCFG-RPPA) for bioinformatics analysis of RPPA data, as well as Samantha McIntosh, Kerry Ardley, Susan Jackson, Lauren Dawes, Stephanie Le, Katherine Papastratos and Qerime Mundrea at the Peter MacCallum

Cancer Centre, Rachel Ridgway at the Beatson Institute for Cancer Research, and Derek Scarborough at the European Cancer Stem Cell Research Centre for their technical assistance.

Figure legends

Figure 1. *PIK3CA* somatic mutation and amplification frequency in prostate cancer. (A) Histogram displaying *PIK3CA* mutation and copy number amplification/gain frequency across 9 prostate cancer genomic datasets. Pie charts show the distribution of primary and metastatic samples for each genomic dataset. (B) Schematic diagram of p110α illustrating mutation frequency across the 9 prostate cancer datasets analysed in relation to the core functional domains. Codons with frequent missense mutations at common hotspots are labelled magenta. To our knowledge, the 4 genetic alterations in light grey text have not been previously reported in other human malignancies, and their impact on p110α function is unknown. p85 = PI3K p85 regulatory subunit binding domain; RBD = RAS binding domain; C2 = calcium-dependent phospholipid-binding domain; Helical = PI3K helical domain; Kinase = PI3/4-kinase domain; aa = amino acid. (C) Kaplan-Meier plot comparing the survival probability of *PIK3CA* mutation and/or amplification/gain carriers with *PIK3CA* unaltered patients within the TCGA provisional prostate cancer patient dataset. *PIK3CA* age-adjusted COXPH HR: 0.55, *P=0.023*.

Figure 2. Heterozygous *Pik3ca*^{H1047R} oncogenic mutation causes invasive prostate cancer in mice that does not phenocopy *Pten*-deletion. (A) Representative H&E images of *Wt,* *Pik3ca*$^{+/HR}$ and *Pten*$^{fl/fl}$ dorsolateral prostate epithelium (scale bar: 100 μm). (B) Histogram displaying phenotype incidence in *Wt,* *Pik3ca*$^{+/HR}$ and *Pten*$^{fl/fl}$ dorsolateral prostate. DLP = dorsolateral prostate, PIN = prostate intraepithelial neoplasia. (C) Bar chart displaying total prostate weight normalised to body weight for *Wt,* *Pik3ca*$^{+/HR}$ and *Pten*$^{fl/fl}$ mice. n = as indicated

(N). Error bars: SEM, *P<0.05 compared to *Wt*, one-way ANOVA with Tukey's multiple comparison test.

Figure 3. *Pten* deletion triggers mTORC2 signaling to facilitate rapid prostate cancer progression relative to *Pik3ca*^{H1047R} mutation. (A) IHC to detect the proliferation marker PCNA in *Wt*, *Pik3ca*$^{+/HR}$ and *Pten*$^{fl/fl}$ prostate carcinoma at 400 d of age (scale bar: 50 μm). (B) Quantitation of PCNA-positive nuclei in *Wt*, *Pik3ca*$^{+/HR}$ and *Pten*$^{fl/fl}$ prostate epithelium (n=3, *P<0.05 compared to *Wt*, or as indicated, one-way ANOVA with Tukey's multiple comparison test. Error bars: SEM). (C) Representative IHC images to detect PTEN, mTORC1 signaling components (p-AKT Thr308, p-RPS6 Ser235/236 and p-4E-BP1 Thr37/46) and mTORC2 substrates (p-AKT Ser473 and p-NDRG1 Thr346) in *Wt* dorsolateral prostate and *Pik3ca*$^{+/HR}$ and *Pten*$^{fl/fl}$ prostate carcinoma at 400 d of age (n=3, scale bar: 50 μm, insert scale bar: 10 μm). IHC quantitation for (D) p-AKT Thr308, (E) p-RPS6 Ser235/236, (F) p-4E-BP1 Thr37/46, (G) p-AKT Ser473 and (H) p-NDRG1 Thr346 in *Wt* dorsolateral prostate and *Pik3ca*$^{+/HR}$ and *Pten*$^{fl/fl}$ prostate carcinoma at 400 d of age (n=3, Error bars: SEM, *P< 0.05 compared to *Wt*, or as indicated, one-way ANOVA with Tukey's multiple comparison correction).

Figure 4. *Pik3ca*$^{+/HR}$ prostate cancer is p110α-dependent, whereas *Pten*$^{fl/fl}$ prostate cancer is p110α and p110β co-dependent. Representative IHC images to detect (A) p-ERK Thr202/Tyr204 and (B) Active RAC1-GTP in *Wt* dorsolateral prostate and *Pik3ca*$^{+/HR}$ and *Pten*$^{fl/fl}$ prostate carcinoma at 400 d of age (n=3, Low magnification scale bar: 100 μm, high magnification scale bar: 10 μm). Bar chart indicating total prostate weight normalised to body weight for *Pik3ca*$^{+/HR}$ mice (C) and *Pten*$^{fl/fl}$ mice (D) with prostate carcinoma administered with either vehicle, p110α-specific inhibitor (A66), p110β-specific inhibitor (TGX-221), pan-PI3K inhibitor (BKM120) or A66 + TGX-221 for 4 weeks compared to age-matched *Wt* controls. n

= as indicated (N). Error bars: SEM, *P<0.05 compared to vehicle, one-way ANOVA with Tukey's multiple comparison correction, ns = not significant. (E) Histogram displaying phenotype incidence for dorsolateral prostate from *Pik3ca*$^{+/HR}$ and *Pten*$^{fl/fl}$ mice treated with either vehicle, p110α-specific inhibitor (A66), p110β-specific inhibitor (TGX-221), pan-PI3K inhibitor (BKM120) or A66 + TGX-221 for 4 weeks.

Figure 5. *Pik3ca* mutation and *Pten* loss cooperate to accelerate prostate cancer progression in mice by upregulating proliferation and mTORC1/2 signaling. (A) Representative IHC images of *Pik3ca*$^{+/HR}$;*Pten*$^{fl/fl}$ prostate carcinoma at 56 and 100 d of age (scale bar: 100 μm). (B) Phenotype incidence histogram for *Wt,* *Pik3ca*$^{+/HR}$, *Pten*$^{fl/fl}$ and *Pik3ca*$^{+/HR}$;*Pten*$^{fl/fl}$ dorsolateral prostate at 56 and 100 d of age. (C) IHC to detect PCNA in *Pik3ca*$^{+/HR}$, *Pten*$^{fl/fl}$ and *Pik3ca*$^{+/HR}$;*Pten*$^{fl/fl}$ stage-matched prostate carcinomas (scale bar: 50 μm). IHC quantitation for (D) PCNA, (E) p-AKT Thr308, (F) p-RPS6 Ser235/236, (G) p-4E-BP1 Thr37/46, (H) p-AKT Ser473 and (I) p-NDRG1 Thr346 in *Pik3ca*$^{+/HR}$, *Pten*$^{fl/fl}$ and *Pik3ca*$^{+/HR}$;*Pten*$^{fl/fl}$ stage-matched prostate carcinomas (n=3, *P<0.05 compared to *Pik3ca*$^{+/HR}$ or as indicated, one-way ANOVA with Tukey's correction. Error bars: SEM). (J) RNA *in situ* hybridisation analysis of *Pik3ca* and *Pik3cb* transcripts in *Pik3ca*$^{+/HR}$, *Pten*$^{fl/fl}$ and *Pik3ca*$^{+/HR}$;*Pten*$^{fl/fl}$ stage-matched prostate carcinomas (n=3, scale bar: 50 μm, insert scale bar: 5 μm). Quantitation of (K) *Pik3ca* and (L) *Pik3cb* mRNA molecules detected by *in situ* hybridisation in *Pik3ca*$^{+/HR}$, *Pten*$^{fl/fl}$ and *Pik3ca*$^{+/HR}$;*Pten*$^{fl/fl}$ stage-matched prostate carcinomas (n=3, *P<0.05 compared to *Wt*, one-way ANOVA with Tukey's correction. Error bars: SEM).

Figure 6. *Pik3ca*$^{+/HR}$ and *Pten*$^{fl/fl}$ prostate cancers acquire CRPC, while *Pik3ca*$^{+/HR}$;*Pten*$^{fl/fl}$ compound mutants display innate resistance to castration. (A) Bar chart displaying total prostate weight normalised to body weight for *Pik3ca*$^{+/HR}$ and *Pten*$^{fl/fl}$ mice 2 and 10 weeks

post-castration relative to age-matched/uncastrated controls. n = as indicated (N). Error bars: SEM, *P<0.05, one-way ANOVA with Tukey's correction. (B) Representative H&E images of *Pik3ca*$^{+/HR}$ and *Pten*$^{fl/fl}$ uncastrated dorsolateral prostate, and 2 and 10 weeks post-castration (scale bar: 100 μm). (C) Representative H&E images of *Pik3ca*$^{+/HR}$*;Pten*$^{fl/fl}$ uncastrated dorsolateral prostate and 2 weeks post-castration (scale bar: 100 μm, n = 5). (D) Bar chart displaying total prostate weight normalised to body weight for *Pik3ca*$^{+/HR}$*:Pten*$^{fl/fl}$ mice 2 weeks post-castration relative to age-matched/uncastrated controls (Error bars: SEM, P=0.3394, unpaired, two-tailed t-test, n = 5). IHC quantitation for (E) PCNA and (F) Cleaved-Caspase 3 (CC3) in *Pik3ca*$^{+/HR}$, *Pten*$^{fl/fl}$ and *Pik3ca*$^{+/HR}$*;Pten*$^{fl/fl}$ dorsolateral prostate 2 weeks post-castration compared to uncastrated/age-matched controls. Error bars: SEM, *P<0.05, one-way ANOVA with Tukey's correction, n = 3. Mice were castrated when prostate carcinoma was prevalent; *Pik3ca*$^{+/HR}$ = 400 d old, *Pten*$^{fl/fl}$ = 200 d old and *Pik3ca*$^{+/HR}$*;Pten*$^{fl/fl}$ =100 d old.

Figure 7. ***De novo* CRPC in *Pik3ca*$^{+/HR}$*;Pten*$^{fl/fl}$ double transgenic animals correlates with NDRG1 inactivation.** Quantitation of IHC to detect mTORC1 signaling components (A) p-AKT Thr308, (B) p-RPS6 Ser235/236, (C) p-4E-BP1 Thr37/46, (D) p-AKT Ser473 and (E) p-NDRG1 Thr346 in *Pik3ca*$^{+/HR}$, *Pten*$^{fl/fl}$ and *Pik3ca*$^{+/HR}$*;Pten*$^{fl/fl}$ prostate tissue 2 weeks post-castration compared to uncastrated, age-matched controls (n = 3, Error bars: SEM, *P<0.05, one-way ANOVA with Tukey's multiple comparison correction). (F) Representative IHC images of p-NDRG1 Thr346 in *Pik3ca*$^{+/HR}$, *Pten*$^{fl/fl}$ and *Pik3ca*$^{+/HR}$*;Pten*$^{fl/fl}$ prostate tissue 2 weeks post-castration compared to uncastrated, age-matched controls (scale bar: 50 μm, n = 3). (G) RPPA analysis was performed on lysates from *Pik3ca*$^{+/HR}$, *Pten*$^{fl/fl}$ and *Pik3ca*$^{+/HR}$*;Pten*$^{fl/fl}$ prostate tissue 2 weeks post-castration, and compared to uncastrated, age-matched controls. Heatmap represents Log2 normalised and median centred data (means of

duplicates, n = 3 per cohort). Mice were castrated when prostate carcinoma was prevalent; $Pik3ca^{+/HR}$ = 400 d old, $Pten^{fl/fl}$ = 200 d old and $Pik3ca^{+/HR}$;$Pten^{fl/fl}$ =100 d old.

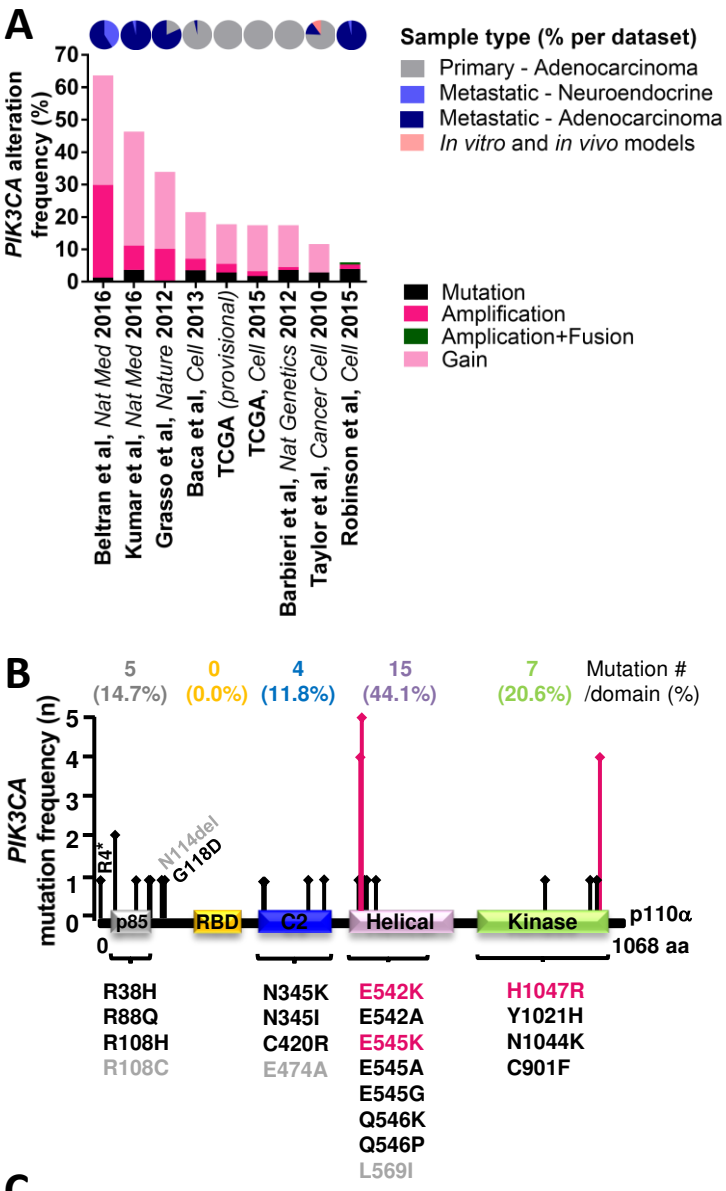
A
Sample type (% per dataset)
Primary - Adenocarcinoma
Metastatic - Neuroendocrine
Metastatic - Adenocarcinoma
In vitro and in vivo models
PIK3CA alteration frequency (%)
70
60
50
40
30
20
10
0
Mutation
Amplification
Amplication+Fusion
Gain
Beltran et al, Nat Med 2016
Kumar et al, Nat Med 2016
Grasso et al, Nature 2012
Baca et al, Cell 2013
TCGA (provisional)
TCGA, Cell 2015
Barbieri et al, Nat Genetics 2012
Taylor et al, Cancer Cell 2010
Robinson et al, Cell 2015

B
5 (14.7%)
0 (0.0%)
4 (11.8%)
15 (44.1%)
7 (20.6%)
Mutation # /domain (%)
PIK3CA mutation frequency (n)
5
4
3
2
1
0
R4*
N114del
G118D
p85
RBD
C2
Helical
Kinase
p110α
0
1068 aa
R38H
R88Q
R108H
R108C
N345K
N345I
C420R
E474A
E542K
E542A
E545K
E545A
E545G
Q546K
Q546P
L569I
H1047R
Y1021H
N1044K
C901F

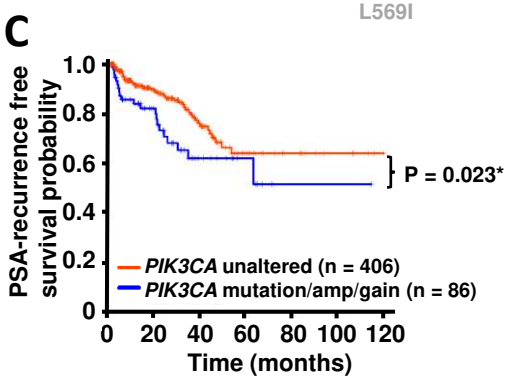
C
PSA-recurrence free survival probability
1.0
0.8
0.6
0.4
0.2
0
P = 0.023*
PIK3CA unaltered (n = 406)
PIK3CA mutation/amp/gain (n = 86)
0
20
40
60
80
100
120
Time (months)

Figure 1

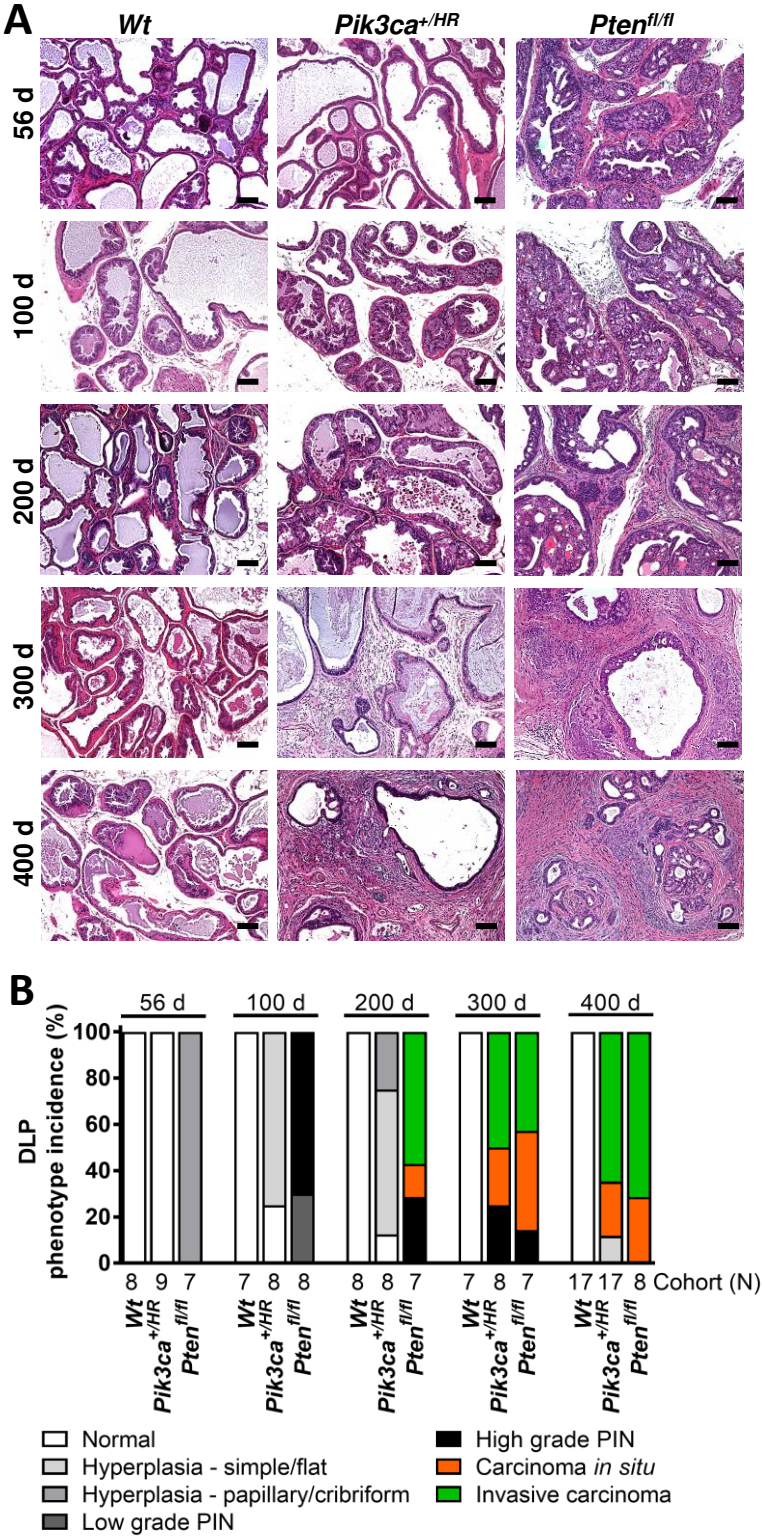
A
Wt
Pik3ca+/HR
Ptenfl/fl
56 d
100 d
200 d
300 d
400 d
B
56 d
100 d
200 d
300 d
400 d
DLP phenotype incidence (%)
100
80
60
40
20
0
8 9 7 7 8 8 8 8 7 7 8 7 17 17 8 Cohort (N)
Wt
Pik3ca+/HR
Ptenfl/fl
Normal
Hyperplasia - simple/flat
Hyperplasia - papillary/cribriform
Low grade PIN
High grade PIN
Carcinoma in situ
Invasive carcinoma
C
Wt
Pik3ca+/HR
Ptenfl/fl
Total prostate weight (% body)
10
8
6
4
2
1.0
0.8
0.6
0.4
0.2
0.0
56
100
200
300
400
Age (days)

Figure 2

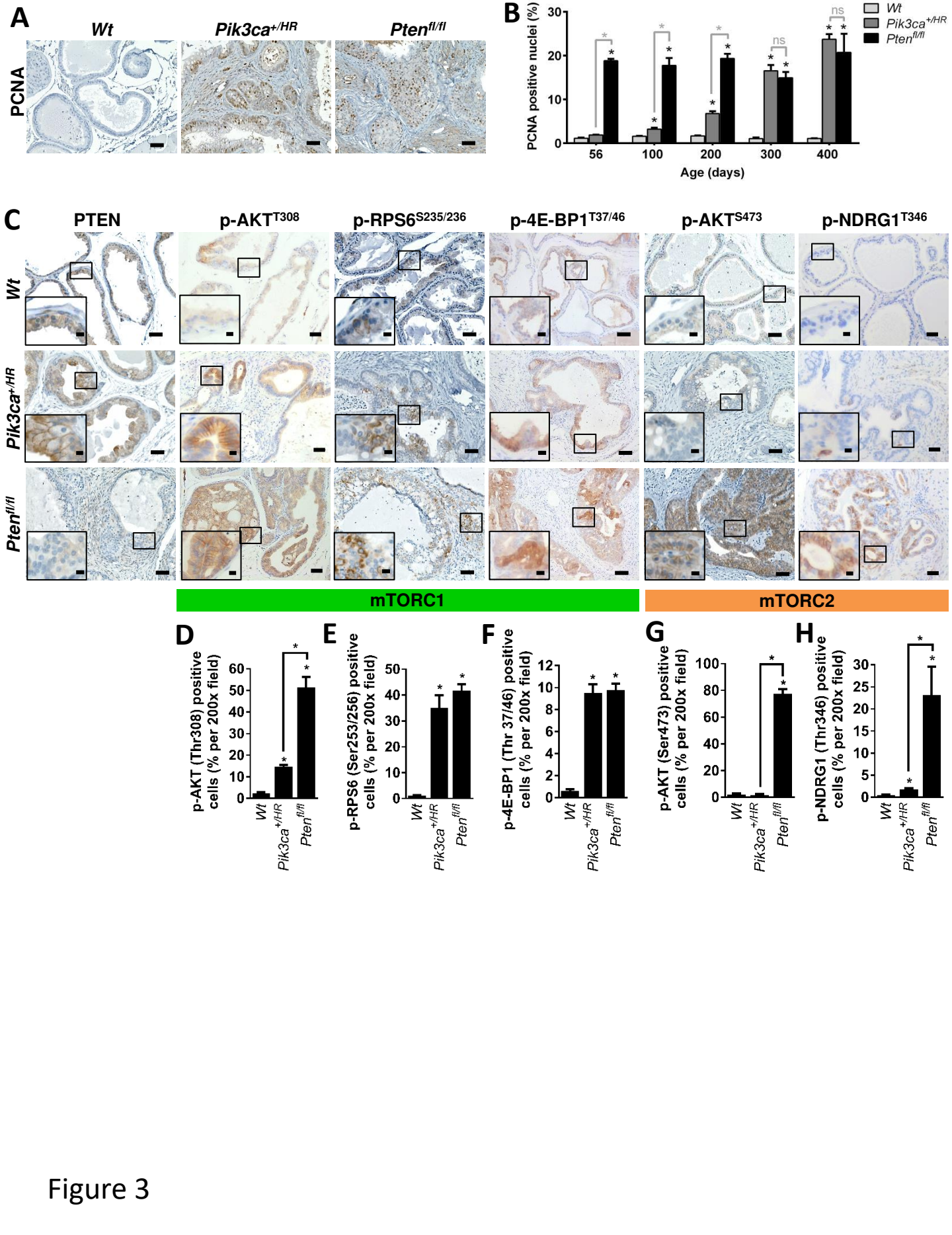
A
Wt
Pik3ca+/HR
Ptenfl/fl
PCNA
B
PCNA positive nuclei (%)
Age (days)
56
100
200
300
400
ns
Wt
Pik3ca+/HR
Ptenfl/fl
C
PTEN
p-AKTT308
p-RPS6S235/236
p-4E-BP1T37/46
p-AKTS473
p-NDRG1T346
Wt
Pik3ca+/HR
Ptenfl/fl
mTORC1
mTORC2
D
p-AKT (Thr308) positive cells (% per 200x field)
E
p-RPS6 (Ser253/256) positive cells (% per 200x field)
F
p-4E-BP1 (Thr 37/46) positive cells (% per 200x field)
G
p-AKT (Ser473) positive cells (% per 200x field)
H
p-NDRG1 (Thr346) positive cells (% per 200x field)

Figure 3

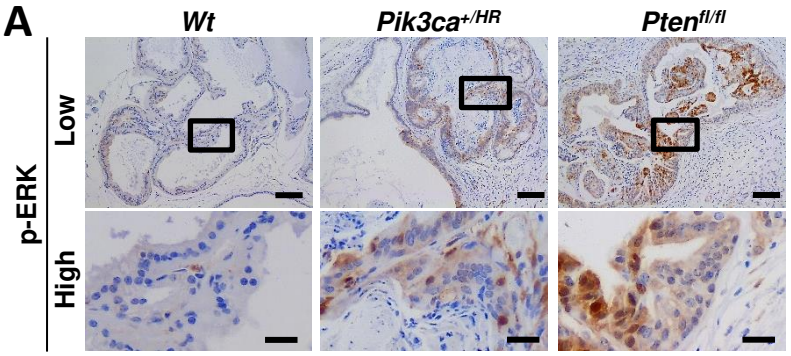
A
Wt
Pik3ca+/HR
Ptenfl/fl
p-ERK
Low
High

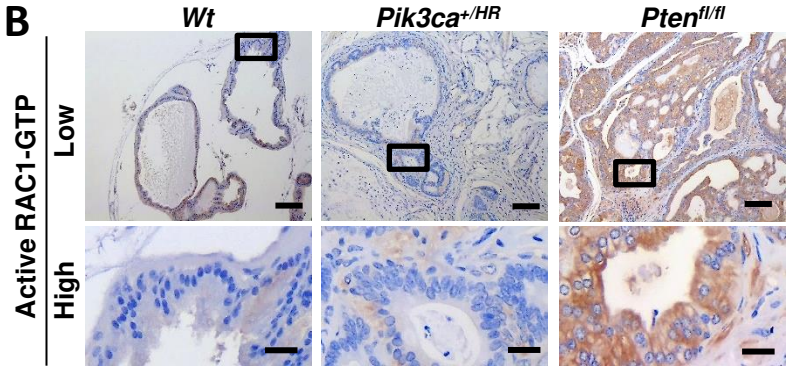
B
Wt
Pik3ca+/HR
Ptenfl/fl
Active RAC1-GTP
Low
High

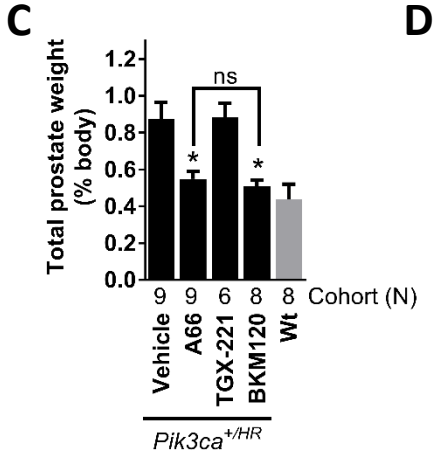
C
Total prostate weight (% body)
1.2
1.0
0.8
0.6
0.4
0.2
0.0
ns
*
*
9 9 6 8 8 Cohort (N)
Vehicle
A66
TGX-221
BKM120
Wt
Pik3ca+/HR

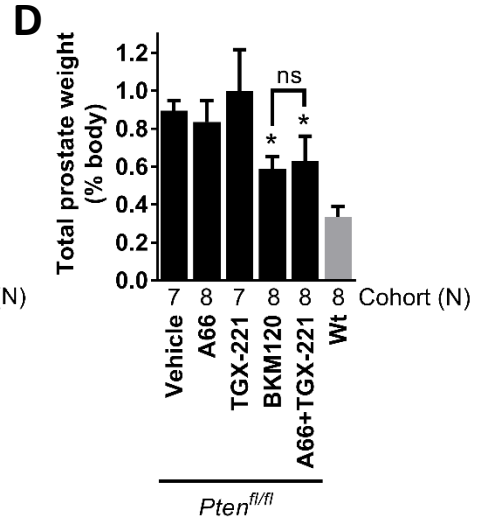
D
Total prostate weight (% body)
1.2
1.0
0.8
0.6
0.4
0.2
0.0
ns
*
*
7 8 7 8 8 8 Cohort (N)
Vehicle
A66
TGX-221
BKM120
A66+TGX-221
Wt
Ptenfl/fl

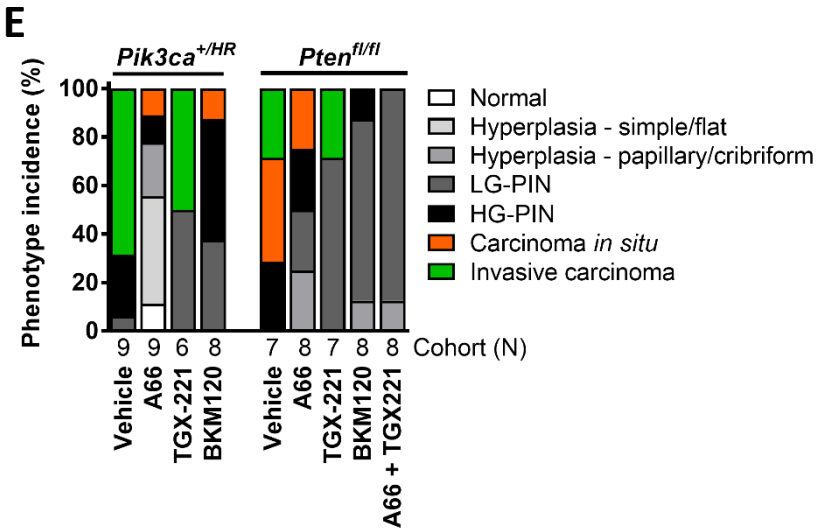
E
Pik3ca+/HR
Ptenfl/fl
Phenotype incidence (%)
100
80
60
40
20
0
Normal
Hyperplasia - simple/flat
Hyperplasia - papillary/cribriform
LG-PIN
HG-PIN
Carcinoma in situ
Invasive carcinoma
9 9 6 8 7 8 7 8 8 Cohort (N)
Vehicle
A66
TGX-221
BKM120
Vehicle
A66
TGX-221
BKM120
A66 + TGX221

Figure 4

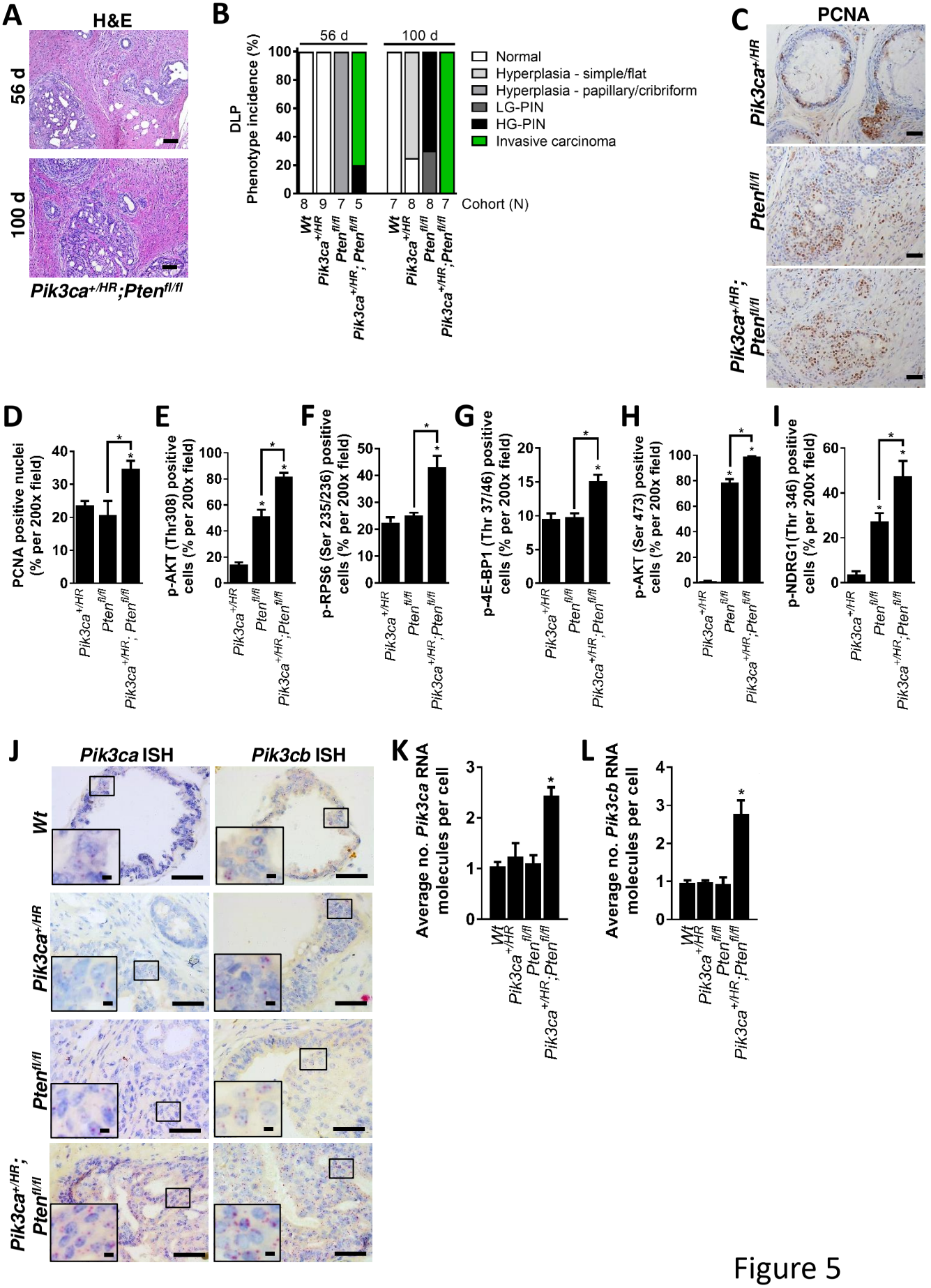
A
H&E
56 d
100 d
Pik3ca+/HR;Ptenfl/fl
B
56 d
100 d
DLP
Phenotype incidence (%)
Normal
Hyperplasia - simple/flat
Hyperplasia - papillary/cribriform
LG-PIN
HG-PIN
Invasive carcinoma
8 9 7 5
7 8 8 7
Cohort (N)
Wt
Pik3ca+/HR
Ptenfl/fl
Pik3ca+/HR;Ptenfl/fl
C
PCNA
Pik3ca+/HR
Ptenfl/fl
Pik3ca+/HR; Ptenfl/fl
D
PCNA positive nuclei (% per 200x field)
E
p-AKT (Thr308) positive cells (% per 200x field)
F
p-RPS6 (Ser 235/236) positive cells (% per 200x field)
G
p-4E-BP1 (Thr 37/46) positive cells (% per 200x field)
H
p-AKT (Ser 473) positive cells (% per 200x field)
I
p-NDRG1(Thr 346) positive cells (% per 200x field)
J
Pik3ca ISH
Pik3cb ISH
Wt
Pik3ca+/HR
Ptenfl/fl
Pik3ca+/HR; Ptenfl/fl
K
Average no. Pik3ca RNA molecules per cell
L
Average no. Pik3cb RNA molecules per cell

Figure 5

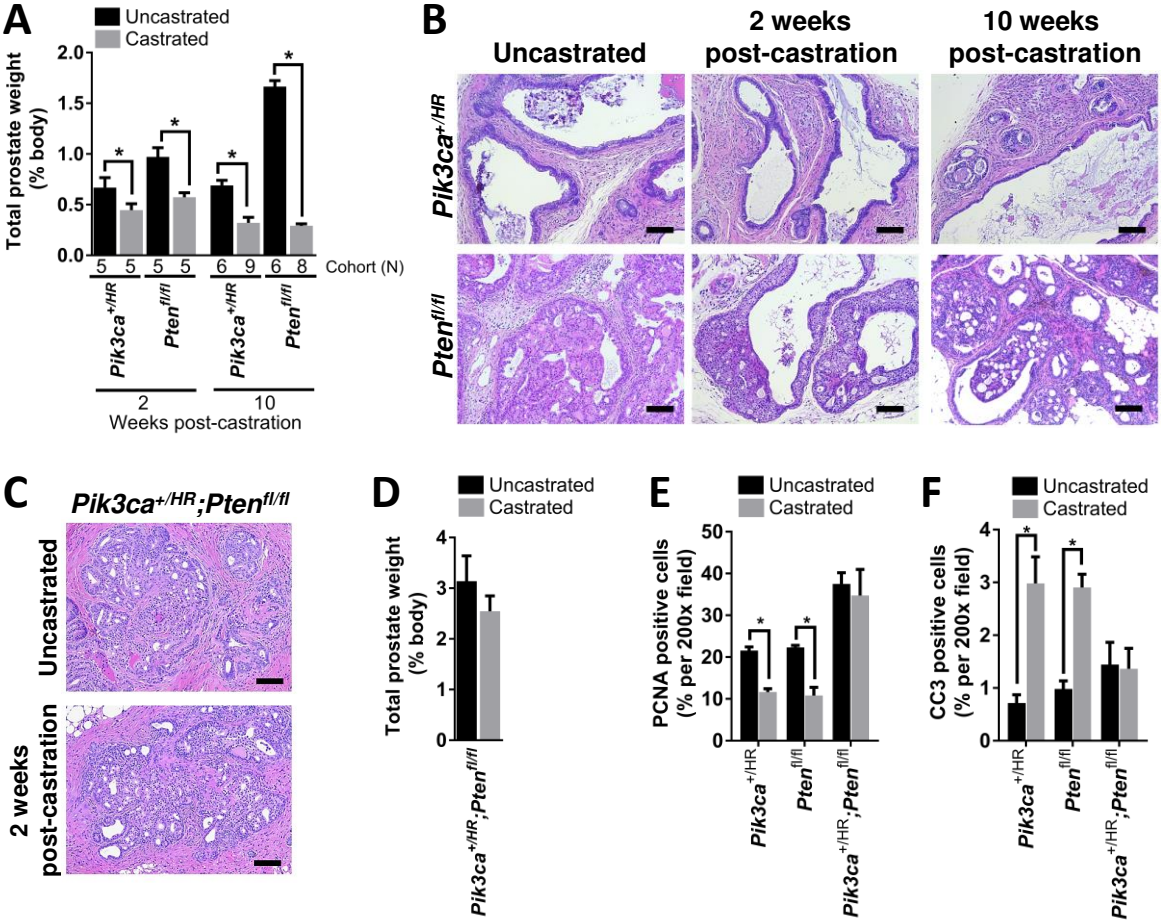
A
Uncastrated
Castrated
Total prostate weight (% body)
2.0
1.5
1.0
0.5
0.0
5 5 5 5 6 9 6 8
Cohort (N)
Pik3ca+/HR
Ptenfl/fl
Pik3ca+/HR
Ptenfl/fl
2
10
Weeks post-castration
B
Uncastrated
2 weeks post-castration
10 weeks post-castration
Pik3ca+/HR
Ptenfl/fl
C
Pik3ca+/HR;Ptenfl/fl
Uncastrated
2 weeks post-castration
D
Uncastrated
Castrated
Total prostate weight (% body)
4
3
2
1
0
Pik3ca+/HR;Ptenfl/fl
E
Uncastrated
Castrated
PCNA positive cells (% per 200x field)
50
40
30
20
10
0
Pik3ca+/HR
Ptenfl/fl
Pik3ca+/HR;Ptenfl/fl
F
Uncastrated
Castrated
CC3 positive cells (% per 200x field)
4
3
2
1
0
Pik3ca+/HR
Ptenfl/fl
Pik3ca+/HR;Ptenfl/fl

Figure 6

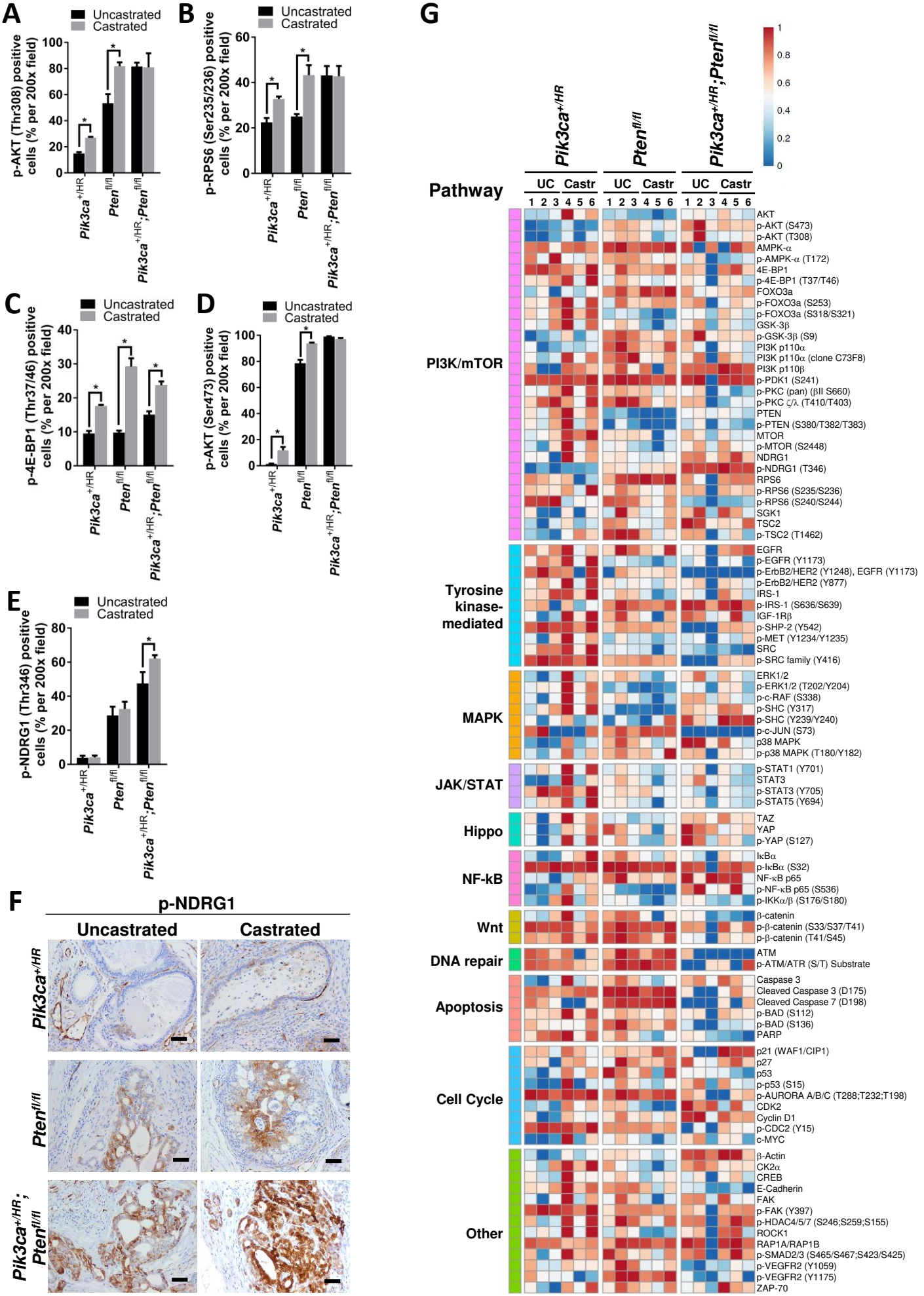
A
Uncastrated
Castrated
p-AKT (Thr308) positive cells (% per 200x field)
Pik3ca+/HR
Ptenfl/fl
Pik3ca+/HR;Ptenfl/fl
B
p-RPS6 (Ser235/236) positive cells (% per 200x field)
C
p-4E-BP1 (Thr37/46) positive cells (% per 200x field)
D
p-AKT (Ser473) positive cells (% per 200x field)
E
p-NDRG1 (Thr346) positive cells (% per 200x field)
F
p-NDRG1
Uncastrated
Castrated
G
Pik3ca+/HR
Ptenfl/fl
Pik3ca+/HR;Ptenfl/fl
UC
Castr
Pathway
PI3K/mTOR
AKT
p-AKT (S473)
p-AKT (T308)
AMPK-α
p-AMPK-α (T172)
4E-BP1
p-4E-BP1 (T37/T46)
FOXO3a
p-FOXO3a (S253)
p-FOXO3a (S318/S321)
GSK-3β
p-GSK-3β (S9)
PI3K p110α
PI3K p110α (clone C73F8)
PI3K p110β
p-PDK1 (S241)
p-PKC (pan) (βII S660)
p-PKC ζ/λ (T410/T403)
PTEN
p-PTEN (S380/T382/T383)
MTOR
p-MTOR (S2448)
NDRG1
p-NDRG1 (T346)
RPS6
p-RPS6 (S235/S236)
p-RPS6 (S240/S244)
SGK1
TSC2
p-TSC2 (T1462)
Tyrosine kinase-mediated
EGFR
p-EGFR (Y1173)
p-ErbB2/HER2 (Y1248), EGFR (Y1173)
p-ErbB2/HER2 (Y877)
IRS-1
p-IRS-1 (S636/S639)
IGF-1Rβ
p-SHP-2 (Y542)
p-MET (Y1234/Y1235)
SRC
p-SRC family (Y416)
MAPK
ERK1/2
p-ERK1/2 (T202/Y204)
p-c-RAF (S338)
p-SHC (Y317)
p-SHC (Y239/Y240)
p-c-JUN (S73)
p38 MAPK
p-p38 MAPK (T180/Y182)
JAK/STAT
p-STAT1 (Y701)
STAT3
p-STAT3 (Y705)
p-STAT5 (Y694)
Hippo
TAZ
YAP
p-YAP (S127)
NF-kB
IκBα
p-IκBα (S32)
NF-κB p65
p-NF-κB p65 (S536)
p-IKKα/β (S176/S180)
Wnt
β-catenin
p-β-catenin (S33/S37/T41)
p-β-catenin (T41/S45)
DNA repair
ATM
p-ATM/ATR (S/T) Substrate
Apoptosis
Caspase 3
Cleaved Caspase 3 (D175)
Cleaved Caspase 7 (D198)
p-BAD (S112)
p-BAD (S136)
PARP
Cell Cycle
p21 (WAF1/CIP1)
p27
p53
p-p53 (S15)
p-AURORA A/B/C (T288;T232;T198)
CDK2
Cyclin D1
p-CDC2 (Y15)
c-MYC
Other
β-Actin
CK2α
CREB
E-Cadherin
FAK
p-FAK (Y397)
p-HDAC4/5/7 (S246;S259;S155)
ROCK1
RAP1A/RAP1B
p-SMAD2/3 (S465/S467;S423/S425)
p-VEGFR2 (Y1059)
p-VEGFR2 (Y1175)
ZAP-70

Figure 7